Royal Netherlands
Meteorological Institute
Ministry of Infrastructure
and Water Management

Maximum Entropy Parameterization of Unresolved Scales in a Two-Layer Quasi-Geostrophic Model

J. Camphuijsen

KNMI Internal report IR-2018-02

Maximum Entropy Parameterization of Unresolved Scales in a Two-Layer Quasi-Geostrophic Model

Jaro Camphuijsen
August 10, 2017

Supervised by:
dr. ir. Camiel Severijns
dr. Wim Verkley
dr. Jaap Kaandorp

To be defended for the acquisition of the *Master of Science* degree on:
August 25, 2017

Koninklijk Nederlands
Meteorologisch Instituut
Ministerie van Infrastructuur en Milieu

Universiteit van Amsterdam

Abstract

Modeling turbulence in the atmosphere is essential for day to day weather prediction and for predicting climate change. An idealized but fairly accurate model of the atmosphere can be constructed by stacking multiple fluid layers of uniform density on top of each other. The simplest of such models is the two-layer quasi-geostrophic model, that uses geostrophic balance to get a closed set of evolution equations. As it is computationally impossible to resolve all scales of motion, we need to truncate the model at a certain scale and describe the small scales by parameterization. A parameterization based on the principle of maximum entropy, that was developed by [Verkley et al., 2016], has been implemented and tested on a two-dimensional model. The new parameterization has no tunable parameters, as its dependence on the system is fully determined by the formalism. In this report, the two-layer quasi-geostrophic model and its energy budget are derived. The maximum entropy parameterization is adapted for this system using the constraint of quasi-geostrophic energy conservation in the unresolved scales. The parameterization is analyzed using multiple diagnostics for both short-term deterministic and lon-term statistical performance. The qualitative performance is compared with a conventional increased-viscosity parameterization. In the analysis, a simulation run of double resolution is used as reference.

Acknowledgements

I would like to thank Wim Verkley and Camiel Severijns, my supervisors at the KNMI, for their support, criticism and thorough feedback. I enjoyed working together and I am grateful to have been part of this project. Of course Jaap Kaandorp, my examiner at the UvA, deserves a spot. He led me to this project and was available for an occasional check-up. Then there is my fellow interns, who have been of great help when I was stuck or just needed some distraction. Especially Sem and Evelien, I enjoyed all of the hours we spent together in our small office room. We discussed so many interesting topics we could have written three theses on anthropology, ethics and pedagogy instead of geophysics. Thanks to my brother Frans, who was so kind to give some feedback on my English grammar and to my parents Helma en Martin who traveled all the way from Amsterdam to Soesterberg to take over the household activities from Martha when she was ill, so I could continue working on this project. That brings me, last but not least, to my soul mate and son, Martha and Djaya. You two have been a terrific support during the whole project and especially the last few weeks. While my attention for you faltered and my time at home grew shorter and shorter, I could expect a happy return every single day. I am amazingly happy we found each other and enjoy every moment of us being together. Thank you all!

Contents

Chapter 1

Introduction

The weather has always been a fascination, friend and enemy of mankind. We need the variety of rainy and sunny weather to grow crops, but extremes like storms or droughts can destroy whole communities and infrastructures. The average weather, or climate and the reported rapid change across the globe could potentially be even more harmful. While we have become increasingly skilled in predicting the weather, there are still many problems with current weather and climate models. One of those problems concerns the flow of fluids, like the air in the atmosphere or water in the ocean.

Full understanding of fluid flow, and specifically a definite solution to the Navier-Stokes equations describing this flow, has not been achieved up to this day. The problem lies in the nonlinearity of the equations. This means that a certain scale of flow not only determines its own time evolution but influences other scales as well. Energy is transferred to smaller scales in a process called the energy cascade. The transfer of energy to larger scales is called backscatter. This complexity is at the heart of the phenomenon called turbulence as the flow at small scales becomes highly chaotic and unpredictable because of extreme sensitivity to small perturbations at any scale.

In numerical fluid modeling, as for example in computational geophysics, we can solve the Navier-Stokes equations on a computational grid by integrating each grid cell over time. However the resolution of the grid on which we perform the computations determines the smallest resolved scale and hereby causes a truncation of scales. This truncation introduces an error in the model due to the omission of the smaller scales and their interaction with the resolved scales. The error tends to be largest near the truncation, where the interactions with unresolved scales are strongest.

To account for these lost processes, the smaller scales are often parameterized by an extra term in the equations. This term then serves as replacement of all scales smaller than the computational grid. In general, parameterizations try to represent the interactions upon the larger scales as good as possible while maintaining low computational cost. Numerous methods of parameterization exist, ranging from very simple to complex. One of the simplest parameterizations is increase of viscosity to mimic the energy that is lost at scales near the truncation to unresolved scales. Such simple schemes however do not catch the complex nature of these interactions, for example the process backscatter is often not accounted for by these schemes. More complex parameterization schemes have been found that do capture this feature. For example, methods where the state of the unresolved scales is represented by a probability density function on which stochastic sampling can be applied. The research of [Thuburn et al., 2013] compares several parameterizations of increasing complexity and analyzes the energy transfer across different scales in these parameterized models. It also proposes a scheme to reduce some of the errors in energy transfer that these parameterizations inevitably produce.

A striking property of all of these parameterization schemes is that they have to be tuned to a specific domain and set of system parameters. Parameter tuning is a cumbersome and time consuming practice and it introduces information into the model that should be deduced from previous known states of the model or from measurements. However, in a changing system like our climate we would prefer a parameterization that does not use information from a historic state, as this information could simply be wrong if applied to future states. A new parametrization has been developed by [Verkley et al., 2016] which uses the approach of replacing the unresolved scales of the quantities in the model equation by a probability density function (PDF) and using the expectation value of this PDF to replace the corresponding variable in the original equation. The novel idea of this parameterization is to find this PDF using the principle of maximum information entropy. The principle tells us that, given some prior

information we have, the best we can do to model the current state of knowledge is to maximize information entropy under the constraint that it is in accordance with this prior information. The expression of information entropy as stated by [Jaynes, 2003] was used together with the energy budget of the unresolved scales as additional information constraint. Previous investigation of this new parameterization on a simple two dimensional doubly periodic system has been promising. [Verkley et al., 2016, Zwaal, 2016]
Although we can approximate the atmosphere by a two-dimensional single layer system due to its shallowness, certain characteristics are not represented in such a system. A better description can be given by stacking several thin layers of constant density and incorporating the interactions between these layers. This so called multilayer shallow water model and specifically (serving ourselves an easy implementation) the two-layer version show many physical phenomena that occur in the atmosphere. The synoptic scale of the earth atmosphere is an interesting system to investigate, as this is the largest scale ($\sim$ 1000km) at which we can make the approximation of near geostrophic balance. This balance occurs between the pressure force in the system and the Coriolis force and is responsible for the atmospheric flow along lines of equal pressure that we tend to see on these scales. Still a small contribution of inertia is present and thus the model is called quasi-geostrophic. Using these approximations, we can construct a closed set of equations, enabling us to simulate the time evolution of the flow. The main focus of this research is on expanding the simple application of the parameterization to the more complex two layer quasi-geostrophic model. Because this system contains a potential energy component in its energy budget, the parametrization has to be established again according to the budgets of this system.
In chapter 2of this thesis the two-layer quasi-geostrophic model is explained. Chapter 3 derives expressions for the energy and energy tendency for the model. Chapter 4 is used to convert the model from Cartesian coordinates to wave number space by writing the necessary equations in spectral coefficients. In chapter 5 an in-depth derivation of the maximum entropy parametrization is given for the current model. The various diagnostic techniques and their results are presented in chapter 6. Chapter 7 concludes with the discussion of the results and recommendations for further investigation.

Chapter 2

The model

In this chapter we will sketch a derivation of the two layer quasi-geostrophic model. It serves the purpose of illustrating particular choices of approximations that were made, and thereby as a validation of using this model in the context of large scale geophysical fluid dynamics. This derivation is also a necessary prelude to the derivation of the energy and energy tendency of the system in chapter 3 which are needed for the construction and analysis of the parameterization. The derivations are based on the works of [Vallis, 2006], [Cushman-Roisin and Beckers, 2009] and [Cavallini and Crisciani, 2013]. We start with the Navier-Stokes equations which form the basis of ordinary[1] fluid dynamics. Directly using the three dimensional Navier-Stokes equations to model the atmosphere or ocean would be correct but practically impossible. We can make some approximations to get a set of simpler equations, tailor made for a system with geophysical properties. The first step is to focus on a thin layer, leading to the shallow water equations. Then we add a second immiscible layer of a different density and determine the interactions between the two layers. Finally we work towards a rotating system where on large scales the Coriolis force counteracts pressure forces leading to quasi-geostrophic flow.

2.1 Navier-Stokes equations

The motion of a fluid is described by the Navier-Stokes equations. These equations are in fact applications of Newton's second law to a continuous medium like a fluid. Starting from Newton's second law $\boldsymbol{f} = m\mathbf{a}$ we write the momentum equation for a single fluid volume element.

$$\rho \frac{D\boldsymbol{v}}{Dt} = \boldsymbol{f} \tag{2.1}$$

The material derivative of the three dimensional velocity vector $\frac{D\boldsymbol{v}}{Dt}$ gives the rate of change of the velocity in a parcel of fluid as it flows along due to the current velocity field.

$$\frac{D\boldsymbol{v}}{Dt} = \frac{\partial \boldsymbol{v}}{\partial t} + (\boldsymbol{v} \cdot \nabla)\boldsymbol{v} = \frac{\partial \boldsymbol{v}}{\partial t} + u\frac{\partial \boldsymbol{v}}{\partial x} + v\frac{\partial \boldsymbol{v}}{\partial y} + w\frac{\partial \boldsymbol{v}}{\partial z} \tag{2.2}$$

Equation (2.1) will form the basis for our model, together with the mass continuity equation which tells us that the net flow of mass into our moving parcel is equal to the increase of its density:

$$\frac{\partial \rho}{\partial t} + \nabla \cdot (\rho \boldsymbol{v}) = 0 \qquad \text{or} \qquad \frac{D\rho}{Dt} + \boldsymbol{v} \cdot \nabla \rho = 0 \tag{2.3}$$

The forces $\boldsymbol{f}$ on a unit volume element can be classified into two categories, internal and external forces. The Navier-Stokes equations assume only two internal stress forces:

- **Internal pressure** from surrounding volume elements

$$\mathbf{f_p} = -\nabla p = -\left(\tfrac{\partial p}{\partial x}\hat{\mathbf{i}} + \tfrac{\partial p}{\partial y}\hat{\mathbf{j}} + \tfrac{\partial p}{\partial z}\hat{\mathbf{k}}\right)$$

[1] For a fluid to be ordinary means to be sufficiently dense to be described as a continuum and lacking relativistic speeds and ionized species.

- **Internal friction**, which for most Newtonian fluids can be approximated by [2]

$$\mathbf{f_v} = \rho\nu\nabla^2\boldsymbol{v}$$

External forces arise from the specific domain onto which the Navier-Stokes equations are used. In our case this will be the earth where two well defined forces occur due to the mass and the rotation of the planet[3]. A third term is added to account for other forces that are present in our atmosphere, for example the solar radiation heating up the surface and thereby stirring the air or extra friction due to the earth surface. We use this term to get our system in an equilibrium state since we would lose all of our energy to internal viscosity and small scales without extra forcing.

- **External gravity** per unit volume gives

$$\mathbf{f_g} = -\rho g\hat{\mathbf{k}}$$

- **External Coriolis force** per unit volume gives

$$\mathbf{f_C} = -\rho f(\hat{\mathbf{k}} \times \boldsymbol{v})$$

- **External other forces**, for example external forcing or damping from mechanical or thermal origins [4]

$$\mathbf{f_{F/D}} = \rho\mu(\boldsymbol{F} - \boldsymbol{v})$$

Inserting these forces into (2.1) gives us the Navier-Stokes equations for an ordinary Newtonian fluid on a rotating massive sphere with additional forcing and damping.

$$\frac{D\boldsymbol{v}}{Dt} = -f\hat{\mathbf{k}} \times \boldsymbol{v} - \frac{1}{\rho}\nabla p + \mathbf{g} + \nu\nabla^2\boldsymbol{v} + \mu(\boldsymbol{F} - \boldsymbol{v}) \tag{2.4}$$

$$\frac{D\rho}{Dt} + \rho\nabla \cdot \boldsymbol{v} = 0 \tag{2.5}$$

2.2 Single hydrostatic shallow layer

The atmospheric layer of prime importance for weather and climate prediction is the troposphere. This layer contains 80 percent of the mass and nearly all of the water vapor in the atmosphere. With its thickness of only 12 km, the horizontal length scales are several orders of magnitude larger than the vertical. The same can be said for the ocean which has a depth of 11 km at its deepest point. Due to this asymmetry several approximations can be made and together with the assumption that the fluid is incompressible, this results in the shallow water equations. The approximations that are made to arrive at these equations are listed and applied.

2.2.1 Shallow water approximations

1. **Incompressibility:** It is assumed that the fluid is incompressible by setting the density as a constant in the mass continuity equation and thus neglecting the derivative of the density. This reduces the mass continuity equation 2.5 to:

$$\nabla \cdot \boldsymbol{v} = 0 \tag{2.6}$$

   Incompressibility is in general not true for any fluid and even more so for a gas. The density of the atmosphere for example has a strong height dependence due to gravity as it is compressed under its own weight near the

[2] This is the first order of the more complete approximation $\sum_r (-1)^{2(r+1)}\nu_r\nabla^{2(r+1)}\boldsymbol{u}$. For compressible fluids, this should also contain an internal stress term accounting for the stress inside the volume element due to compression.

[3] Actually both these forces are fictitious forces that are a manifestation of respectively the differential rotation experienced on the earth surface and the curvature of space time. Both can be expressed as a force term when our frame of reference is located on and moving with the earth surface.

[4] The expression given below is not used in real climate models as it is far too simple to account for all the physical, biological and antropogenic processes that occur on the planet. However we only need a simple forcing and damping to keep our system in statistical equilibrium.

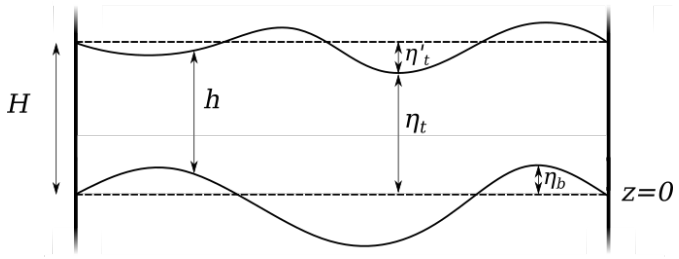

Figure 2.1: Schematic cross section of a single hydrostatic shallow water layer, with its surface and fluid height variables.

surface. While in an ocean model, the approximation of incompressibility is physically sound, we can not say the same for the atmosphere [5]. However even in the case of the atmosphere, we can make the approximation if we assume vertical flow velocities to be relatively small. We can see this if we consider a shallow water column that experiences a net horizontal inflow. This horizontal convergence will exhibit a vertical extension of the water column rather than an increase in density. In chapter 2.3 we will stack an extra layer of different density on top and this can be extended to multiple layers to account for the stratification in the atmosphere.

2. **Hydrostatic:** We can assume the shallow layer to be in hydrostatic equilibrium, meaning that the vertical pressure and gravitational force are in perfect balance.

$$\frac{\partial p}{\partial z} = -\rho g \tag{2.7}$$

3. β**-Plane:** The last assumption is that the Coriolis force linearly depends on the y coordinate so in expression for Coriolis force we get

$$f = f_0 + \beta y \tag{2.8}$$

In this way a space-varying Coriolis force is applied, while the model can still be used on a double periodic domain without introducing discontinuities in the evolution equations as will be shown in chapter 2.3. A Coriolis force that varies in space causes specific physical phenomena, like Rossby waves, that do not occur if the Coriolis parameter is set constant. The physical representation of a β plane domain would be a plane tangent to the earth surface, where the latitude of touching determines the value of β.

2.2.2 Velocity equations

Considering a single layer of fluid, bounded by a top surface η_t and a bottom surface η_b, several height variables can be discerned. Referring to fig. 2.1, we see that we have for the thickness of the layer at a certain location:

$$h(x, y) = \eta_t(x, y) - \eta_b(x, y) \tag{2.9}$$

Because we assume density to be constant and assuming a pressure at the top surface of p_t, the hydrostatic relation in this layer can be integrated to give

$$p(x, y, z) = p_t(x, y) + \rho g(\eta_t(x, y) - z) \tag{2.10}$$

where η is the upper boundary of the fluid surface. We can decouple the horizontal gradient from the vertical. Dropping the explicit dependence of p and η on (x, y) to keep notation uncluttered:

$$\nabla_h = \left(\frac{\partial}{\partial x}\hat{\mathbf{i}} + \frac{\partial}{\partial y}\hat{\mathbf{j}}\right) \tag{2.11}$$

$$\nabla p = \frac{\partial p}{\partial z}\hat{\mathbf{k}} + \nabla_h p = -\rho g\hat{\mathbf{k}} + \nabla_h(p_t + \rho g\eta_t) \tag{2.12}$$

[5] Using instead the assumption of constant potential temperature $\theta = T\left(\frac{p_r}{p}^{\kappa}\right)$, where p is the pressure, p_r a reference pressure and κ a dimensionless parameter, we can in fact construct a model very similar to the shallow water equations as shown by [Verkley, 2000]. This model is applicable to the troposphere and in the same way as the shallow water equations results in horizontal flow being constant in the vertical direction.

We see that the assumption of hydrostatic balance causes the horizontal pressure gradient to be independent of height. This implies that also the horizontal velocity does not depend on height and that we can express the evolution of horizontal velocity, which we will denote by $\boldsymbol{u}$, independent of the vertical coordinate. We insert (2.12) into (2.4) to get the shallow water momentum equation for viscid flow in terms of the horizontal velocity vector $\boldsymbol{u}$. Note how the assumption of hydrostatic equilibrium lets the gravity and the vertical component of the pressure force in equation (2.4) cancel out. We will drop the subscript h in the horizontal gradient.

$$\frac{\partial \boldsymbol{u}}{\partial t} + (\boldsymbol{u} \cdot \nabla)\boldsymbol{u} = -(f_0 + \beta y)\hat{\mathbf{k}} \times \boldsymbol{u} - \nabla(\frac{p_t}{\rho} + g\eta_t) + \nu\nabla^2\boldsymbol{u} + \mu(\boldsymbol{F} - \boldsymbol{v}) \tag{2.13}$$

Furthermore we can split the reduced mass continuity equation (2.6) into a horizontal and vertical component and integrate from the bottom to the top of the fluid. Where we use that $\eta_t - \eta_b = h$ and that the vertical velocity at position $w(x, y, z)$ is the material derivative of the vertical position z of the fluid element at that position.

$$\begin{aligned} & \int_h \left(\frac{\partial w(x,y,z)}{\partial z} + \nabla \cdot \boldsymbol{u} \right) dz = 0 \\ \Rightarrow \quad & w(\eta_t) - w(\eta_b) + h\nabla \cdot \boldsymbol{u} = 0 \\ \Rightarrow \quad & \frac{D}{Dt}(\eta_t - \eta_b) + h\nabla \cdot \boldsymbol{u} = \frac{Dh}{Dt} + h\nabla \cdot \boldsymbol{u} = 0 \end{aligned} \tag{2.14}$$

Equation (2.14) can also be explained by the logical consequence of incompressibility, that any net horizontal flux into a fluid column of height h will make this column expand to be able to contain the extra mass. Note how we went from a three dimensional representation in (2.4) with velocity vector $\boldsymbol{v} = u\hat{\mathbf{i}} + v\hat{\mathbf{j}} + w\hat{\mathbf{k}}$ to eq. (2.13) that only involves horizontal velocity $\boldsymbol{u} = u\hat{\mathbf{i}} + v\hat{\mathbf{j}}$. The vertical velocity can still be retrieved from the three dimensional continuity eq. (2.5) by integrating over height. If we do this, the vertical velocity turns out to scale linearly with height.

2.2.3 Potential vorticity

It is now convenient to introduce a quantity called the *vorticity*[6], defined as the curl of the horizontal velocity.

$$\boldsymbol{\omega} \equiv \nabla \times \boldsymbol{u} = \left(\frac{\partial v}{\partial x} - \frac{\partial u}{\partial y} \right) \hat{\mathbf{k}} = \zeta \hat{\mathbf{k}} \tag{2.15}$$

Since the vorticity has only a $\hat{\mathbf{k}}$ component, we will use the scalar ζ and call it by the same name. To obtain an evolution equation for the vorticity, we will start by using the vector identity

$$\begin{aligned} (\boldsymbol{u} \cdot \nabla)\boldsymbol{u} =& \tfrac{1}{2}\nabla(\boldsymbol{u}^2) - \boldsymbol{u} \times (\nabla \times \boldsymbol{u}) \\ =& \tfrac{1}{2}\nabla\boldsymbol{u}^2 + (\nabla \times \boldsymbol{u}) \times \boldsymbol{u} \\ =& \tfrac{1}{2}\nabla\boldsymbol{u}^2 + \boldsymbol{\omega} \times \boldsymbol{u} \end{aligned}$$

to write (2.13) as

$$\frac{\partial \boldsymbol{u}}{\partial t} + \boldsymbol{\omega} \times \boldsymbol{u} = -(f_0 + \beta y)\hat{\mathbf{k}} \times \boldsymbol{u} - \nabla(\frac{p_t}{\rho} + g\eta_t + \frac{1}{2}\boldsymbol{u}^2) + \nu\nabla^2\boldsymbol{u} + \mu(\boldsymbol{F} - \boldsymbol{v}) \tag{2.16}$$

$$\frac{\partial \boldsymbol{u}}{\partial t} + (\boldsymbol{\omega} + (f_0 + \beta y)\hat{\mathbf{k}}) \times \boldsymbol{u} = -\nabla(\frac{p_t}{\rho} + g\eta_t + \frac{1}{2}\boldsymbol{u}^2) + \nu\nabla^2\boldsymbol{u} + \mu(\boldsymbol{F} - \boldsymbol{v}) \tag{2.17}$$

To continue, we note the following vector identity, where some terms vanish because we take the divergence of a curl and the fact that $\boldsymbol{u}$ does not vary in the direction of $\boldsymbol{\omega}$.

$$\nabla \times (\boldsymbol{\omega} \times \boldsymbol{u}) = (\boldsymbol{u} \cdot \nabla)\boldsymbol{\omega} - \cancel{(\boldsymbol{\omega} \cdot \nabla)\boldsymbol{u}} + \boldsymbol{\omega}\nabla \cdot \boldsymbol{u} - \cancel{\boldsymbol{u}\nabla \cdot \boldsymbol{\omega}} \tag{2.18}$$

[6] In fact the vorticity is defined for the three dimensional velocity field in a similar way. The quantity we use here is often called the *shallow water vorticity* as it only takes into account the horizontal velocity in systems where the horizontal velocity is independent of the vertical coordinate. We will use the term vorticity to denote this shallow water vorticity and also its scalar variant.

We take the curl of (2.17) and use the above identity and the definition of vorticity, where the whole gradient term cancels because the curl of a gradient is zero.

$$\nabla \times \frac{\partial \boldsymbol{u}}{\partial t} + \nabla \times ((\boldsymbol{\omega} + \boldsymbol{f}) \times \boldsymbol{u}) = \cancel{-\nabla \times \nabla(\frac{p_t}{\rho} + g\eta_t + \frac{1}{2}\boldsymbol{u}^2)} + \nabla \times \nu\nabla^2\boldsymbol{u} + \nabla \times \mu(\boldsymbol{F} - \boldsymbol{v}) \tag{2.19}$$

$$\Rightarrow \quad \frac{\partial \boldsymbol{\omega}}{\partial t} + (\boldsymbol{u} \cdot \nabla)(\boldsymbol{\omega} + \boldsymbol{f}) + (\boldsymbol{\omega} + \boldsymbol{f})\nabla \cdot \boldsymbol{u} = \nu\nabla^2\boldsymbol{\omega} + \mu(\boldsymbol{\omega}_F - \boldsymbol{\omega}) \tag{2.20}$$

$$\Rightarrow \quad \frac{\partial \zeta}{\partial t} + (\boldsymbol{u} \cdot \nabla)(\zeta + f) + (\zeta + f)\nabla \cdot \boldsymbol{u} = \nu\nabla^2\zeta + \mu(\zeta_F - \zeta) \tag{2.21}$$

The next step is to combine this equation with the continuity equation (2.14) by replacing the divergence of the velocity in (2.21). We add the coriolis term to the time derivative, we can do this because the earth rotation is constant in time and therefore the time derivative is zero.

$$\frac{\partial \zeta}{\partial t} + (\boldsymbol{u} \cdot \nabla)(\zeta + f) - \frac{(\zeta + f)}{h}(\frac{\partial h}{\partial t} + \boldsymbol{u} \cdot \nabla h) = \nu\nabla^2\zeta + \mu(\zeta_F - \zeta) \tag{2.22}$$

$$\Rightarrow \quad \frac{1}{h}\frac{\partial}{\partial t}(\zeta + f) + (\boldsymbol{u} \cdot \nabla)\frac{(\zeta + f)}{h} - \frac{(\zeta + f)}{h^2}(\frac{\partial h}{\partial t} + \boldsymbol{u} \cdot \nabla h) = \frac{1}{h}\left(\nu\nabla^2\zeta + \mu(\zeta_F - \zeta)\right) \tag{2.23}$$

$$\Rightarrow \quad \frac{\partial}{\partial t}(\frac{\zeta + f}{h}) + (\boldsymbol{u} \cdot \nabla)(\frac{\zeta + f}{h}) = \frac{1}{h}\left(\nu\nabla^2\zeta + \mu(\zeta_F - \zeta)\right) \tag{2.24}$$

$$\Rightarrow \quad \frac{\partial Q}{\partial t} + \boldsymbol{u} \cdot \nabla Q = \frac{1}{h}\left(\nu\nabla^2\zeta + \mu(\zeta_F - \zeta)\right) \tag{2.25}$$

In the first step we divide by h as to recognize the quotient rule for derivatives in step two. In the third step we defined the quantity Q which we will call the shallow water *potential vorticity*. The potential vorticity will play a crucial role in the rest of the derivations. We actually see from eq. (2.25) that in the absence of friction (i.e. $\nu = 0$) and other forcing terms, the potential vorticity is conserved. The problem we now face is that the relation between $\boldsymbol{u}$ and Q is not unique, so we do not have a closed equation that can be solved in time.

2.3 Two-layer quasi-geostrophic model

Continuing from our newly acquired shallow water potential vorticity equation, we will first introduce the concept of multiple layers and then add a new set of approximations to arrive at the equations for so called quasi-geostrophic flow. Pure geostrophic flow means that the Coriolis force exactly balances the pressure forces so that the flow is along lines of equal pressure. The term "quasi" simply indicates that the Coriolis and pressure force almost balance out, but a small contribution of advection is still present.

2.3.1 Layers

We will start by stacking two shallow water models with constant but different densities on top of each other to obtain a model with discrete layers. This approximation to the actual continuous stratification in the atmosphere is questionable. However, such a model shows many interesting geophysical phenomena while remaining easy to use in calculations. In the following subscripts on the fields will denote the layer index, ζ_1 and ζ_2 being the vorticity of respectively the top layer and bottom layer. A schematic view of this model is given in fig. 2.2. We have for each layer a fluid height $h_n(x, y)$, consisting of a a mean fluid height H_n and deviations from this mean $h'_n(x, y)$. We also assume a flat bottom topography $\eta_b = 0$ and we can define the interface heights η_n and the corresponding interface displacements from the mean. The bottom surface η_2 of layer one is now the top surface of layer two and through this interface, the layers gain a coupling of their flow fields. We can summarize the height variables by:

$$\eta_1(x, y) = h_1(x, y) + h_2(x, y) \qquad \eta_2(x, y) = h_2(x, y) \tag{2.26}$$

$$\eta'_1(x, y) = h'_1(x, y) + h'_2(x, y) \qquad \eta'_2(x, y) = h'_2(x, y) \tag{2.27}$$

Using hydrostatic balance, as we did in eq. (2.10) for the single layer, we can express the pressure for each layer in layer heights η_n, again with a pressure at the top surface p_t. However this time we assume this pressure to be

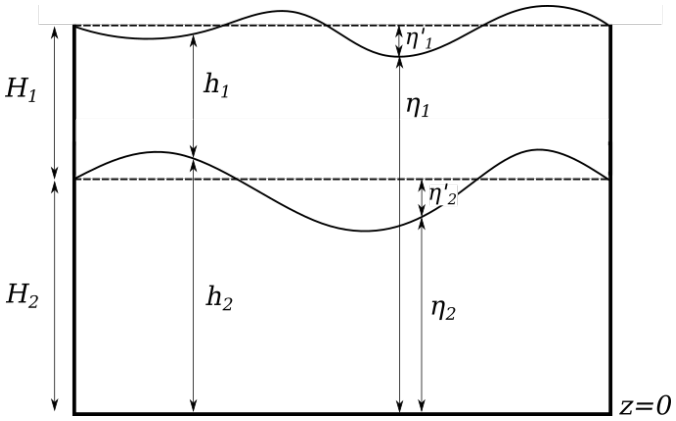

Figure 2.2: Schematic cross section of the two-layer quasi-geostrophic model, with its surface and fluid height variables.

constant[7].

$$p_1(x,y) = p_t + \rho_1 g(\eta_1(x,y) - z) \qquad p_2(x,y) = p_t + \rho_2 g(\eta_2(x,y) - z) + \rho_1 g(h_1(x,y))$$
$$= p_t + \rho_2 g(\eta_2(x,y) - z) + \rho_1 g(\eta_1(x,y) - \eta_2(x,y))$$

Taking the horizontal gradient of these expressions for pressure and dropping the explicit (x, y) dependence of the surface heights to keep notation uncluttered:

$$\nabla p_1 = \rho_1 \nabla g(\eta_1) \qquad \nabla p_2 = g\nabla(\rho_2(\eta_2) + \rho_1(\eta_1 - \eta_2))$$
$$= g\nabla\left(\rho_2(\eta_2) + \rho_2(\eta_1 - \eta_2) + (\rho_1 - \rho_2)(\eta_1 - \eta_2)\right.$$
$$= \rho_2 \nabla \left(g\eta_1 + g'(\eta_2 - \eta_1)\right) \tag{2.28}$$

where $g' = g\frac{\rho_2 - \rho_1}{\rho_2}$ is called the reduced gravity and where we lost the extra pressure term on top, since it is assumed constant. We can write down the potential vorticity and its evolution equation for both layers, similar to (2.25)[8].

$$Q_n = \frac{f + \zeta_n}{h_n} \tag{2.29}$$

$$\frac{\partial Q_n}{\partial t} + \boldsymbol{u} \cdot \nabla Q_n = \frac{1}{h_n}\left(\nu\nabla^2\zeta_n + \mu(\zeta_F + \zeta)\right) \tag{2.30}$$

2.3.2 Quasi-geostrophic potential vorticity

First we will sum up the assumptions that will lead us through the derivation of the quasi-geostrophic equations.

1. **Near-geostrophic:** The advective term is small and the Coriolis force and the pressure force are in approximate balance. We introduce a measure for this balance called the Rossby number(Ro). The Rossby number is defined as the ratio of the typical scale of the advective flow over the scale of the Coriolis term.

$$Ro \equiv \frac{(U^2 L)}{f_0 U} = \frac{U}{fL} \tag{2.31}$$

   Where we have typical scales U, L and f_0 for respectively the velocity, length and Coriolis force[9]. Note that if the Rossby number is zero we recover pure geostrophic flow. For increasing Ro, the effects of the advective term becomes more prominent.

[7] This is a good assumption for layers of fluid with air on top, say the ocean, since the pressure gradient in air is much smaller.

[8] The derivation is similar to the one layer case. The one thing that changes is the pressure expression of the bottom layer as it will also include the pressure exerted by the gravity of the top layer, however the pressure term vanishes when we take the curl in the derivation of the vorticity equation.

[9] Note that we take the constant part of the beta-plane Coriolis force. We already implicitly assume that the variation β is small compared to f_0. In approximation 3 we state this assumption explicitly.

2. $\boldsymbol{L \sim L_d}$ **:** The length scale of the motion is not significantly larger than the deformation scale L_d. The deformation scale is the length scale at which gravitational effects are equally important as effects due to the Coriolis force and is defined by:

$$L_d \equiv \frac{\sqrt{gH}}{f_0} \tag{2.32}$$

For the layered shallow water equations this implies that variations in fluid height are small compared to the total depth.

$$h'_n << H_n \tag{2.33}$$

3. $\boldsymbol{|\beta L| \ll |f_0|}$ **:** Variations of the Coriolis parameter over the length scale of motion are small compared to the scale of the Coriolis parameter itself.

The first approximation is of course central to our model. The second represents a choice of parameter regime[10]. The third approximation is then necessary to get an interesting flow domain[11]. We use the approximations to rewrite the potential vorticity (2.29).

$$Q_n = \frac{f+\zeta_n}{h_n} = \frac{f+\zeta_n}{H_n(1+h'_n/H_n)} \tag{2.34}$$

$$\approx \frac{1}{H_n}(f+\zeta_n)\left(1-\frac{h'_n}{H_n}\right) \qquad \leftarrow \text{2: Small surface variations, } (1+x)^{-1} = 1-x+\mathcal{O}(x^2) \tag{2.35}$$

$$\approx \frac{1}{H_n}\left(f_0+\beta y+\zeta_n-(f_0+\beta y+\cancel{\zeta_n})\frac{h'_n}{H_n}\right) \qquad \leftarrow \text{1: Rossby number is small, } f \gg \zeta_n \tag{2.36}$$

$$\approx \frac{1}{H_n}\left(f_0+\beta y+\zeta_n-(f_0+\cancel{\beta y})\frac{h'_n}{H_n}\right) \qquad \leftarrow \text{3: Variations in Coriolis force are small} \tag{2.37}$$

The constant f_0/H_n has no effect on the evolution equation, and we end up with the quasi-geostrophic potential vorticity:

$$q_n = \beta y + \zeta_n - f_0\frac{h'_n}{H_n} \tag{2.38}$$

This quantity will evolve according to $Dq_n/Dt = 0$ in the absence of viscosity, forcing and damping. To be able to say something about this evolution, however, we need to know how the interface h_n evolves in time. For this we use perfect geostrophic balance to get an expression for the velocity in terms of interface height. Perfect geostrophic flow for our two layers is described by:

$$f_0\hat{\mathbf{k}} \times \boldsymbol{u}_n = -\frac{1}{\rho_n}\nabla p_n \tag{2.39}$$

Inserting eq. (2.28) for the pressure gradients in (2.39) gives an expression for the velocity vectors in terms of surface deviations.

$$f_0\hat{\mathbf{k}} \times \boldsymbol{u}_1 = -g\nabla\eta'_1 \qquad\qquad f_0\hat{\mathbf{k}} \times \boldsymbol{u}_2 = -g\nabla\eta'_1 - g'\nabla(\eta'_2-\eta'_1) \tag{2.40}$$

Where we could switch to the layer depth deviations due to the fact that the layer depths only appear as derivatives and the mean layer depth is of course constant. Next we introduce a useful quantity called the *stream function*, implicitly defined by setting its curl equal to the velocity vector.

$$\boldsymbol{u} = \begin{pmatrix} u \\ v \end{pmatrix} = \begin{pmatrix} -\frac{\partial\psi}{\partial y} \\ \frac{\partial\psi}{\partial x} \end{pmatrix} = \nabla \times \psi \tag{2.41}$$

[10] The alternative, where $L^2 >> L_d^2$, leads us to the so called planetary geostrophic equations which are on earth not applicable to the atmosphere and only to the ocean on very large scales

[11] Choosing β to be of the same order as f_0 would give a situation where only zonal flow (in the x-direction) is present. It has been suggested that the banded pattern on the giant planets in our solar system, like Jupiter, originates from this mechanism.

Using (2.40), we can write this stream function as a function of surface heights.

$$\psi_1 = \frac{g}{f_0}\eta_1' \qquad \psi_2 = \frac{g}{f_0}\eta_1' + \frac{g'}{f_0}(\eta_2' - \eta_1') \tag{2.42}$$

From these we can get an expression for the surface deviations η_n' and finally using (2.27) also the layer height deviations h_n'.

$$\eta_1' = \frac{f_0}{g}\psi_1 \qquad \eta_2' = \frac{f_0}{g}\psi_1 + \frac{f_0}{g'}(\psi_2 - \psi_1) \tag{2.43}$$

$$h_1' = \eta_1' - \eta_2' = \frac{f_0}{g'}(\psi_1 - \psi_1) \qquad h_2' = \eta_2' = \cancel{\frac{f_0}{g}\psi_1} + \frac{f_0}{g'}(\psi_2 - \psi_1) \tag{2.44}$$

The first right hand term in the expression for the second layer in 2.44 is dropped to make the system simpler. This is the assumption of a rigid lid instead of a free surface. The approximation is justified for two immiscible layers that have comparable densities by [Duchene, 2014]. Inserting 2.44 in 2.38 we get the quasi-geostrophic potential vorticity for each layer in terms of the stream function.

$$q_1 = \beta y + \zeta_1 + \Gamma_1(\psi_2 - \psi_1) \tag{2.45a}$$

$$q_2 = \beta y + \zeta_2 + \Gamma_2(\psi_1 - \psi_2) \tag{2.45b}$$

with the interface interaction parameters $\Gamma_n = f_0^2/(g' H_n)$. Using the definition of the stream function (2.41) we can rewrite the advection term of (2.30) as a Jacobian operator.

$$\boldsymbol{u}_n \cdot \nabla q_n = u_n \frac{\partial q_n}{\partial x} + v_n \frac{\partial q_n}{\partial y} = \frac{\partial \psi_n}{\partial x}\frac{\partial q_n}{\partial y} - \frac{\partial \psi_n}{\partial y}\frac{\partial q_n}{\partial x} = \mathcal{J}(\psi_n, q_n) \tag{2.46}$$

This quasi-geostrophic potential vorticty is then advected as follows, when we recover the additional forcing term.

$$\frac{\partial q_n}{\partial t} + J(\psi_n, q_n) = F_n - D_n \tag{2.47}$$

With $F = \mu(\zeta_f - \zeta)$ the forcing term combined with the linear damping term and $D = -\nu\nabla^2\zeta_n$ the dissipation or viscous term. It is in fact useful to take the term including β out of the potential vorticity since it is constant in time and write it explicitly in the evolution equation so we get the following system.

$$q_1' = \zeta_1 + \Gamma_1(\psi_2 - \psi_1) \tag{2.48a}$$

$$q_2' = \zeta_2 + \Gamma_2(\psi_1 - \psi_2) \tag{2.48b}$$

$$\frac{\partial q_n'}{\partial t} + J(\psi_n, q_n') + \beta\frac{\partial \psi_n}{\partial x} = F_n - D_n \tag{2.49}$$

Chapter 3

Conserved quantities

In a two dimensional model with uniform thickness the only type of energy that is of interest is the kinetic energy. Now due to the two layers of different density and a variable interface, we also get a potential energy term (PE) and conversion between potential and kinetic energy will be possible. The total energy of the system, in absence of forcing and damping, remains conserved, but the kinetic energy per layer or as a total is no longer a conserved quantity.

3.1 Kinetic energy

The kinetic energy is in general given by $KE = \frac{1}{2}m\boldsymbol{v}^2$. For a continuous flowing medium we should integrate this quantity over the full domain to account for the variable velocity field. In our two layer model we find for each layer a kinetic energy of[1]:

$$\begin{aligned} \mathrm{KE}_n =& \frac{1}{2}\rho_n \int_0^{2\pi}\int_0^{2\pi}\int_0^{H_n} \boldsymbol{u}_n^2 \, dx\, dy\, dz && (3.1)\\ =& -\frac{1}{2}\rho_n H_n \int_0^{2\pi}\int_0^{2\pi} \psi_n \zeta_n \, dx\, dy && (3.2) \end{aligned}$$

In the second equality we have made use of the definition of the stream function and the product rule:

$$\begin{aligned} \boldsymbol{u}^2 =& \nabla\psi \cdot \nabla\psi && (3.3)\\ =& \cancel{\nabla\cdot(\psi\nabla\psi)} - \psi\nabla^2\psi && (3.4) \end{aligned}$$

Where the first term on the right hand side cancels due to Gauss' theorem and the periodic boundary conditions. In the same way it can be shown that for the derivative of the kinetic energy we get a similar expression.

$$\begin{aligned} \frac{d}{dt}\mathrm{KE}_n =& \rho_n \int_0^{2\pi}\int_0^{2\pi}\int_0^{H_n} \boldsymbol{u}_n \frac{\partial \boldsymbol{u}_n}{\partial t} \, dx\, dy\, dz && (3.5)\\ =& -\rho_n H_n \int_0^{2\pi}\int_0^{2\pi} \psi_n \frac{\partial \zeta_n}{\partial t} \, dx\, dy && (3.6) \end{aligned}$$

3.2 Available potential energy

Subsequently we investigate how to set up an expression for the potential energy. Since we have incompressible fluids, the only candidate is gravity. For gravitational potential energy we write in general $PE = mgh$, where h is relative to a certain reference height on which the potential energy is defined zero. The system of two immiscible

[1] It turns out that, in a hydrostatic layer, we only need to consider the kinetic energy associated with the horizontal velocity field $\boldsymbol{u}$. Note that this field is independent of height within the layer.

fluids has lowest energy when the interface is flat and therefore situated at H_2, with the fluid of lowest density on top. We let this be our reference state and define the *available potential energy* (APE) to be the potential energy minus that of the reference state. This time we will integrate over the full domain, including both layers. Note that the assumptions of a flat bottom and rigid lid on top are reflected by the integration domains.

$$\text{APE} = \int_0^{2\pi}\int_0^{2\pi}\left(\int_0^{H_2+h_2'} g\rho_2 z\,dz + \int_{H_2+h_2'}^{H_1+H_2} g\rho_1 z\,dz\right)dx\,dy \tag{3.7}$$

$$-\int_0^{2\pi}\int_0^{2\pi}\left(\int_0^{H_2} g\rho_2 z\,dz + \int_{H_2}^{H_1+H_2} g\rho_1 z\,dz\right)dx\,dy \tag{3.8}$$

$$=\int_0^{2\pi}\int_0^{2\pi} g(H_2h_2' + \frac{1}{2}(h_2')^2)(\rho_2-\rho_1)\,dx\,dy \tag{3.9}$$

$$=g\frac{1}{2}(\rho_2-\rho_1)\int_0^{2\pi}\int_0^{2\pi}(h_2')^2\,dx\,dy \tag{3.10}$$

$$=\frac{\rho_2 f_0^2}{2g'}\int_0^{2\pi}\int_0^{2\pi}(\psi_2-\psi_1)^2\,dx\,dy \tag{3.11}$$

Where in the second step we used that integrating all interface height deviations (h_2') over the horizontal domain must be zero due to the conservation of mass. In the third step we inserted the expression of h_2' in terms of the stream function from eq. (2.44). We can also show that for the time derivative of the available potential energy we get:

$$\frac{d}{dt}\text{APE} = \frac{\rho_2 f_0^2}{2g'}\int_0^{2\pi}\int_0^{2\pi}\frac{\partial}{\partial t}(\psi_2-\psi_1)^2\,dx\,dy \tag{3.12}$$

$$=\frac{\rho_2 f_0^2}{2g'}\int_0^{2\pi}\int_0^{2\pi}2(\psi_2-\psi_1)\frac{\partial}{\partial t}\left(\psi_2-\psi_1\right)\,dx\,dy \tag{3.13}$$

$$=\frac{\rho_2 f_0^2}{g'}\int_0^{2\pi}\int_0^{2\pi}-\psi_1\frac{\partial}{\partial t}\left(\psi_2-\psi_1\right)-\psi_2\frac{\partial}{\partial t}\left(\psi_1-\psi_2\right)\,dx\,dy \tag{3.14}$$

3.3 Total energy

We decide to make the approximation[2] $\rho_1 = \rho_2 = \frac{\rho_1+\rho_2}{2}$, which is true if the density difference between the layers is relatively small. So adding up up all energy contributions we get from (3.6) and (3.14):

$$\begin{aligned}E_{tot} =& KE_1 + KE_2 + APE\\ =&\int_0^{2\pi}\int_0^{2\pi}-\frac{1}{2}\rho_1 H_1\psi_1\zeta_1 - \frac{1}{2}\rho_2 H_2\psi_2\zeta_2 + \frac{\rho_2 f_0^2}{2g'}(\psi_2-\psi_1)^2\,dx\,dy\\ =&\frac{C}{2}\int_0^{2\pi}\int_0^{2\pi}-\frac{1}{\Gamma_1}\psi_1\zeta_1 - \frac{1}{\Gamma_2}\psi_2\zeta_2 + (\psi_2(\psi_2-\psi_1)-\psi_1(\psi_2-\psi_1))\,dx\,dy \qquad (3.15)\\ =&\frac{C}{2}\int_0^{2\pi}\int_0^{2\pi}\left(-\frac{1}{\Gamma_1}\psi_1\zeta_1 - \psi_1(\psi_2-\psi_1)\right)dx\,dy + \int_0^{2\pi}\int_0^{2\pi}\left(-\frac{1}{\Gamma_2}\psi_2\zeta_2 - \psi_2(\psi_1-\psi_2)\right)dx\,dy\\ =&-\frac{C}{2}\int_0^{2\pi}\int_0^{2\pi}\left(\frac{1}{\Gamma_1}\psi_1 q_1' + \frac{1}{\Gamma_2}\psi_2 q_2'\right)dx\,dy \qquad (3.16)\end{aligned}$$

where we have defined $C = \frac{f_0^2}{g'}\frac{\rho_1+\rho_2}{2}$. We recognize in the last step that, using (2.48), we can express the total energy in terms of the reduced potential vorticity and the stream functions. Even though we have made some

[2]This approximation can be made because of some of the approximations we made before in our derivation. For example the rigid lid approximation is bound to distort the energy budget.

approximations in the derivation of the energy, we can show that the quantity (3.16) is conserved by taking the time derivative of expression eq. (3.15).

$$\begin{aligned}\frac{dE_{tot}}{dt} =&\frac{C}{2}\int_0^{2\pi}\int_0^{2\pi} -\frac{1}{\Gamma_1}\left(\frac{\partial\psi_1}{\partial t}\zeta_1 + \psi_1\frac{\partial}{\partial t}\zeta_1\right) - \frac{1}{\Gamma_2}\left(\frac{\partial\psi_2}{\partial t}\zeta_2 + \psi_2\frac{\partial}{\partial t}\zeta_2\right)\\ &+\left(\frac{\partial\psi_2}{\partial t}(\psi_2-\psi_1) + \psi_2\frac{\partial}{\partial t}(\psi_2-\psi_1) - \frac{\partial\psi_2}{\partial t}(\psi_2-\psi_1) - \psi_2\frac{\partial}{\partial t}(\psi_2-\psi_1)\right)\\ =&\frac{C}{2}\int_0^{2\pi}\int_0^{2\pi} -\frac{2}{\Gamma_1}\psi_1\frac{\partial\zeta_1}{\partial t} - \frac{2}{\Gamma_2}\psi_2\frac{\partial\zeta_2}{\partial t} + 2\left(\psi_2\frac{\partial}{\partial t}(\psi_2-\psi_1) - \psi_1\frac{\partial}{\partial t}(\psi_2-\psi_1)\right)\\ =&C\int_0^{2\pi}\int_0^{2\pi} -\frac{1}{\Gamma_1}\psi_1\frac{\partial q_1'}{\partial t} - \frac{1}{\Gamma_2}\psi_2\frac{\partial q_2'}{\partial t} = C\int_0^{2\pi}\int_0^{2\pi} -\frac{1}{\Gamma_1}\psi_1\frac{\partial q_1}{\partial t} - \frac{1}{\Gamma_2}\psi_2\frac{\partial q_2}{\partial t}\end{aligned} \tag{3.17}$$

Where we use that $\frac{\partial\psi_n}{\partial t}\zeta_n = \frac{\partial\psi_n}{\partial t}\nabla^2\psi_n = \frac{\partial\nabla^2\psi_n}{\partial t}\psi_n = \frac{\partial\zeta_n}{\partial t}\psi_n$. Also note that the β term in the potential vorticity is constant in time and therefore does not contribute to the energy budget. Since we only have the time derivative of q_n', we can choose to replace it with q_n to obtain the last expression. When we insert the potential evolution equation (2.47) into eq. (3.17) we see that the Jacobian vanishes due to the product with ψ_n, the integration over a periodic domain (enabling the interchange of the Jacobian operator $\psi_n\mathcal{J}(\psi_n, q_n) = \mathcal{J}(\psi_n, \psi_n)q_n$) and the fact that the Jacobian of two equal fields is zero. Therefore we are only left with an integration over the viscosity and forcing term, which is exactly the energy conservation statement: in absence of friction and external forcing, the energy is conserved.

$$\begin{aligned}\frac{dE_{tot}}{dt} =&C\int_0^{2\pi}\int_0^{2\pi} -\frac{1}{\Gamma_1}\psi_1\frac{\partial q_1}{\partial t} - \frac{1}{\Gamma_2}\psi_2\frac{\partial q_2}{\partial t}\\ =&C\int_0^{2\pi}\int_0^{2\pi} -\sum_{n=\{1,2\}}\frac{1}{\Gamma_n}\psi_n\big(\mu(\zeta_f-\zeta) + \nu\nabla^2\zeta_n\big)\end{aligned} \tag{3.18}$$

3.4 Potential enstrophy

We introduce another quantity that is conserved in the model and that can be used as diagnostic to compare different parameterizations. It is called potential enstrophy and can be seen as a measure of rotational kinetic energy. We see from the evolution equation (2.30) that, without forcing and dissipation, the potential vorticity q_n is a materially conserved quantity. Because potential vorticity is a conserved quantity, any function of q_n is conserved as well. The conservation of potential enstrophy can be derived in a similar way as energy conservation from the evolution equation, this time multiplying by q_n.

$$\frac{dZ_n}{dt} = 0, \qquad Z = \frac{1}{2}\int_0^{2\pi}\int_0^{2\pi} q_n^2\,dx\,dy$$

Note that, unlike the energy, the enstrophy is conserved within each layer as well as in the whole system. In fact, because potential vorticity is conserved, any arbitrary function of potential vorticity $f(q_n)$ is also conserved. Enstrophy is just one of the infinite number of conserved quantities in the system.

Chapter 4

Spectral representation

For the parameterization of our model it is convenient to expand the streamfunction and potential vorticity as an infinite series of complex exponentials. Advantages of this representation are that a propagating wave can be solved exactly and that the analysis becomes easier. At the base of these advantages is the fact that when using the spectral representation, calculating the spatial derivatives becomes very easy. We will start in section 4.1 by defining the space of spectral modes and their derivatives and introduce notation. In section 4.2 we will derive the potential vorticity for a single mode in terms of ζ and define the transformation matrix to be able to switch between q and ζ. Next we will write down the potential vorticity equations for both layers in section 4.3. This chapter will conclude with the expression of energy and energy tendency in spectral coefficients, needed for the parameterization and diagnostics.

4.1 Basis functions and derivatives

Using a general Fourier series, we can express any two dimensional field, for example the vorticity ζ_n, as:

$$\zeta_n = \sum_{\boldsymbol{k}} \zeta_{n,\boldsymbol{k}}(t) Y_{\boldsymbol{k}}(x,y) = \sum_{\mathbf{k}\in\mathcal{T}} \zeta_{n,\boldsymbol{k}} e^{i\boldsymbol{k}\boldsymbol{x}} = \sum_{k_x}\sum_{k_y} \zeta_{n,k_x k_y} e^{ik_x x} e^{ik_y y}, \tag{4.1}$$

where the combined wave number $\boldsymbol{k}$ is in the vector space $\mathcal{T}$ consisting of all possible wave numbers with components k_x and k_y. Similar expansions can be made for q_n and ψ_n, using corresponding coefficients $q_{n,\boldsymbol{k}}$ and $\psi_{n,\boldsymbol{k}}$. The functions $Y_{\boldsymbol{k}}$ are orthonormal with respect to the inner product

$$(\xi,\chi) = \left(\frac{1}{2\pi}\right)^2 \int_0^{2\pi}\int_0^{2\pi} \xi(x,y)^* \chi(x,y)\,\mathrm{d}x\mathrm{d}y, \tag{4.2}$$

which is, they satisfy $(Y_{\boldsymbol{k}}, Y_{\boldsymbol{k}'}) = \delta_{\boldsymbol{k}\boldsymbol{k}'}$, with δ the Kronecker delta. Due to this orthonormality the coefficients $\zeta_{n,\boldsymbol{k}}$ can be calculated by the inner products

$$\zeta_{n,\boldsymbol{k}} = (Y_{\boldsymbol{k}}, \zeta_n) = \left(\frac{1}{2\pi}\right)^2 \int_0^{2\pi}\int_0^{2\pi} Y^*_{\boldsymbol{k}} \zeta_n\,\mathrm{d}x\mathrm{d}y \tag{4.3}$$

The spectral coefficients of the spatial derivatives of a field can be calculated by the inner product of the derivative of the field

$$\begin{aligned}
\left(\left(\frac{\partial}{\partial x}\right)^p\left(\frac{\partial}{\partial y}\right)^q\psi\right)_{\boldsymbol{k}} &= \left(Y_{\boldsymbol{k}}, \left(\frac{\partial}{\partial x}^p\frac{\partial}{\partial y}^q\psi\right)\right) \\
&= \left(\frac{1}{2\pi}\right)^2\int_0^{2\pi}\int_0^{2\pi} e^{-ik_x x}e^{-ik_y y}\left(\frac{\partial}{\partial x}\right)^p\left(\frac{\partial}{\partial y}\right)^q\sum_{k'_x}\sum_{k'_y}\psi_{k'_x k'_y}e^{ik'_x x}e^{ik'_y y}\,\mathrm{d}x\mathrm{d}y \\
&= \left(\frac{1}{2\pi}\right)^2\int_0^{2\pi}\int_0^{2\pi} e^{-ik_x x}e^{-ik_y y}\sum_{k'_x}\sum_{k'_y}(ik'_x)^p(ik'_y)^q\psi_{\boldsymbol{k}'}e^{ik'_x x}e^{ik'_y y}\,\mathrm{d}x\mathrm{d}y \\
&= (ik_x)^p(ik_y)^q\psi_{\boldsymbol{k}} \qquad (4.4)
\end{aligned}$$

Here we see the primary reason for formulating the model in spectral coefficients. The spatial derivative becomes a simple multiplication by the corresponding wave number. In particular the spectral coefficients of the vorticity are given, using (2.41) in terms of the streamfunction by:

$$\zeta_{\boldsymbol{k}} = (\nabla^2\psi)_{\boldsymbol{k}} = \left(\left(\frac{\partial}{\partial x}\right)^2\psi + \left(\frac{\partial}{\partial y}\right)^2\psi\right)_{k_x k_y} = -(k_x^2+k_y^2)\psi_{k_x k_y} = -\boldsymbol{k}^2\psi_{\boldsymbol{k}}. \qquad (4.5)$$

4.2 Potential vorticity transformation

We saw in eq. (2.45) that we can express the quasi-geostrophic potential vorticity in terms of relative vorticity and the stream function. When we go to a spectral representation, it can be easily shown that the expression for potential vorticity still holds.

$$q_{1,\boldsymbol{k}} = (\beta y)_{\boldsymbol{k}} + \zeta_{1,\boldsymbol{k}} + \Gamma_1(\psi_{2,\boldsymbol{k}} - \psi_{1,\boldsymbol{k}}) \qquad (4.6)$$

$$q_{2,\boldsymbol{k}} = (\beta y)_{\boldsymbol{k}} + \zeta_{2,\boldsymbol{k}} + \Gamma_2(\psi_{1,\boldsymbol{k}} - \psi_{2,\boldsymbol{k}}) \qquad (4.7)$$

The same is true for the reduced potential vorticity in (2.48):

$$q'_{1,\boldsymbol{k}} = \zeta_{1,\boldsymbol{k}} + \Gamma_1(\psi_{2,\boldsymbol{k}} - \psi_{1,\boldsymbol{k}}) \qquad (4.8)$$

$$q'_{2,\boldsymbol{k}} = \zeta_{2,\boldsymbol{k}} + \Gamma_2(\psi_{1,\boldsymbol{k}} - \psi_{2,\boldsymbol{k}}) \qquad (4.9)$$

Using these equations we can write out a transformation matrix for the relation between $q'_{n,\boldsymbol{k}}$ and $\zeta_{n,\boldsymbol{k}}$:

$$\begin{bmatrix} q'_{1,\mathbf{k}} \\ q'_{2,\mathbf{k}} \end{bmatrix} = \begin{bmatrix} 1+\frac{\Gamma_1}{\mathbf{k}^2} & -\frac{\Gamma_1}{\mathbf{k}^2} \\ -\frac{\Gamma_2}{\mathbf{k}^2} & 1+\frac{\Gamma_2}{\mathbf{k}^2} \end{bmatrix}\begin{bmatrix} \zeta_{1,\mathbf{k}} \\ \zeta_{2,\mathbf{k}} \end{bmatrix} \qquad (4.10)$$

$$\begin{bmatrix} \zeta_{1,\mathbf{k}} \\ \zeta_{2,\mathbf{k}} \end{bmatrix} = \frac{1}{\mathrm{Det}(\mathbf{M})}\begin{bmatrix} 1+\frac{\Gamma_2}{\mathbf{k}^2} & \frac{\Gamma_1}{\mathbf{k}^2} \\ \frac{\Gamma_2}{\mathbf{k}^2} & 1+\frac{\Gamma_1}{\mathbf{k}^2} \end{bmatrix}\begin{bmatrix} q'_{1,\mathbf{k}} \\ q'_{2,\mathbf{k}} \end{bmatrix} \qquad (4.11)$$

4.3 Vorticity equation

All terms of the evolution equation for reduced vorticity (2.49) can now be written in their spectral representation.

$$\begin{aligned}
\frac{\partial q_n}{\partial t} &= \sum_{\boldsymbol{k}\in\mathcal{T}}\frac{\partial q_{n,\boldsymbol{k}}}{\partial t}Y_{\boldsymbol{k}} \\
J(\psi_n, q_n) &= \sum_{\boldsymbol{k}\in\mathcal{T}}(J(\psi_n,q_n))_{\boldsymbol{k}}Y_{\boldsymbol{k}} \\
\frac{\partial\psi_n}{\partial x} &= -\sum_{\boldsymbol{k}\in\mathcal{T}}\frac{ik_x}{\boldsymbol{k}^2}\zeta_{n,\boldsymbol{k}}Y_{\boldsymbol{k}} \\
\nabla^2\zeta_n &= -\sum_{\boldsymbol{k}\in\mathcal{T}}\boldsymbol{k}^2\zeta_{n,\boldsymbol{k}}Y_{\boldsymbol{k}}
\end{aligned}$$

We adapt a somewhat strange notation for the spectral coefficients of the Jacobian term. This is due to the fact that the Jacobian itself is an operator and we mean to obtain the spectral coefficients of the field that this operator produces. However, the Jacobian operation is still performed in grid space. Thus to compute the Jacobian term in spectral space we first need to transform the spectral fields $\psi_{n,\boldsymbol{k}}$ and $q_{n,\boldsymbol{k}}$ to their grid space representation using (4.1), then evaluate the Jacobian and finally transform the result back to spectral space using (4.3)[1]. Even though we need two Fourier transforms to switch between physical and spectral space and back again, this approach is considerably faster than doing the operation in spectral space, as was conceived by [Orszag, 1970]. We get the time evolution of a reduced potential vorticity coefficient $q'_{n\boldsymbol{k}}$, by taking the inner product with the basis function $Y_{\boldsymbol{k}}$.

$$\frac{\partial q'_{n,\boldsymbol{k}}}{\partial t} = -J(\psi_n, q'_n)_{\boldsymbol{k}} - \frac{ik_x}{\boldsymbol{k}^2}\zeta_{n,\boldsymbol{k}} + \mu(\zeta_f - \zeta) - \boldsymbol{k}^2\zeta_{n,\boldsymbol{k}} \tag{4.12}$$

This equation tells us, given coefficients $\zeta_{n,\boldsymbol{k}}$ and $q'_{n,\boldsymbol{k}}$ at a certain time, the change of the coefficient $\partial q'_{n,\boldsymbol{k}}$ after a time step ∂t. It can be implemented, using the transformation matrices (4.10) and (4.11) to relate $\zeta_{n,\boldsymbol{k}}$ and $q'_{n,\boldsymbol{k}}$.

[1] Actually, before transforming the fields to grid space, first the necessary derivatives to compute the Jacobian are obtained, as this is very easy in spectral space. These derivative fields are then transformed to grid space. The Jacobian operation then only consists of multiplications and subtraction of these fields.

Chapter 5

Parameterization

To construct a computer model, the infinite sums in the previous section must be truncated, leaving a region of resolved modes ($\mathcal{R}$) and unresolved modes ($\mathcal{U}$). However, any truncation will lead to errors in the model's behaviour and thus we need to modify the evolution equation to counteract these errors. This is called the parameterization of the unresolved scales and can be done in several ways. A simple, yet conventional approach is to increase the viscosity, with the idea of draining extra energy from mainly the small scales. However, [Thuburn et al., 2013] shows that this may have adverse effects. Due to the large amount of energy that is present in the large scales compared to the small scales, the increased viscosity also has the largest impact at the large scales. We will nevertheless use this approach to compare our own parameterization with. Our own parameterization belongs to a class of parameterizations where the unresolved scales are replaced by a probability density function (PDF). What distinguishes this new parameterization from others in the same class, is how the PDF is obtained, namely using the principle of maximum information entropy. The derivations given here will follow the line of reasoning of [Verkley et al., 2016]. First the equations will be decomposed into a resolved and unresolved part in section 5.1. Next the principle of maximum entropy will be introduced. From maximizing the expression for information entropy, a probability density function for the spectral coefficients of the flow field is derived in section 5.2. Finally in section 5.3 the functional form of the obtained PDF is exploited to get the expectation value , which is then inserted into the model equations.

5.1 Decomposition

Evolution equation

First we decompose our fields ζ_n, ψ_n and q_n in resolved and unresolved modes $\zeta_n^{\mathcal{R}}$ and $\zeta_n^{\mathcal{U}}$ etc. As we want an expression for the evolution of these fields we need to decompose eq. (2.47) which contains a Jacobian matrix so that we also discern the resolved $J^{\mathcal{R}}$ and unresolved $J^{\mathcal{U}}$ parts of the Jacobian[1]. Then we decompose the potential vorticity evolution equation into a resolved and unresolved part and for the direct computation of the resolved states we get:

$$\frac{dq_n^{\mathcal{R}}}{dt} + J^{\mathcal{R}}(\psi_n^{\mathcal{R}} + \psi_n^{\mathcal{U}}, q_n^{\mathcal{R}} + q_n^{\mathcal{U}}) = \nu\nabla\zeta_n^{\mathcal{R}} + \mu(F_n^{\mathcal{R}} - \zeta_n^{\mathcal{R}}) \tag{5.1}$$

$$\frac{dq_n^{\mathcal{U}}}{dt} + J^{\mathcal{U}}(\psi_n^{\mathcal{R}} + \psi_n^{\mathcal{U}}, q_n^{\mathcal{R}} + q_n^{\mathcal{U}}) = \nu\nabla\zeta_n^{\mathcal{U}} + \mu(F_n^{\mathcal{U}} - \zeta_n^{\mathcal{U}}) \tag{5.2}$$

Equation (5.2) will not be evaluated as it concerns the evolution of unresolved modes. In eq. (5.1) we still have a contribution from the unresolved scales in the Jacobian term, here we see the nonlinearity of the problem at hand. By truncating the model we lose this contribution and it is the task of a parameterization to replace it. Our approach of parameterization is to assume that the unresolved coefficients can be represented by a probability

[1]Formally, in the decomposition of the Jacobian we use the notation $J^{\mathcal{U}}(...)$ to represent the operation $P^{\mathcal{U}}J(...)$ where P is an orthogonal projection operator that projects upon the unresolved subspace $\mathcal{U}$ of all basis functions in terms of which ζ, ψ and q are represented, $J^{\mathcal{R}}$ is defined correspondingly for the resolved domain.

density function. The exact deterministic evolution will be lost by the transition to a stochastic function. However the statistical characteristics of the flow evolution should be conserved.

$$\left\langle \frac{dq_n^{\mathcal{R}}}{dt} \right\rangle + \left\langle J^{\mathcal{R}}(\psi_n^{\mathcal{R}} + \psi_n^{\mathcal{U}}, q_n^{\mathcal{R}} + q_n^{\mathcal{U}}) \right\rangle = \left\langle \nu \nabla \zeta_n^{\mathcal{R}} \right\rangle + \left\langle \mu(F_n^{\mathcal{R}} - \zeta_n^{\mathcal{R}}) \right\rangle \tag{5.3}$$

To get definite values for the computer model from the stochastic function, we could sample the distribution as for example investigated by [Crommelin and Verheul, 2016]. We will take the simpler approach of determining the expectation value of the distribution (5.3). For the purely resolved terms the expectation value equals the term itself since these can be explicitly computed. The Jacobian can be expanded to give[2]

$$\begin{aligned}
\left\langle J^{\mathcal{R}}\left(\psi_n^{\mathcal{R}} + \psi_n^{\mathcal{U}}, q_n^{\mathcal{R}} + q_n^{\mathcal{U}}\right)\right\rangle &= \left\langle J^{\mathcal{R}}\left(\psi_n^{\mathcal{R}}, q_n^{\mathcal{R}}\right)\right\rangle + \left\langle J^{\mathcal{R}}\left(\psi_n^{\mathcal{R}}, q_n^{\mathcal{U}}\right)\right\rangle + \left\langle J^{\mathcal{R}}\left(\psi_n^{\mathcal{U}}, q_n^{\mathcal{R}}\right)\right\rangle + \left\langle J^{\mathcal{R}}\left(\psi_n^{\mathcal{U}}, q_n^{\mathcal{U}}\right)\right\rangle \\
&= J^{\mathcal{R}}\left(\psi_n^{\mathcal{R}}, q_n^{\mathcal{R}}\right) + J^{\mathcal{R}}\left(\psi_n^{\mathcal{R}}, \left\langle q_n^{\mathcal{U}}\right\rangle\right) + J^{\mathcal{R}}\left(\left\langle \psi_n^{\mathcal{U}}\right\rangle, q_n^{\mathcal{R}}\right) + \left\langle J^{\mathcal{R}}\left(\psi_n^{\mathcal{U}}, q_n^{\mathcal{U}}\right)\right\rangle \\
&= J^{\mathcal{R}}\left(\psi_n^{\mathcal{R}} + \left\langle \psi_n^{\mathcal{U}}\right\rangle, q_n^{\mathcal{R}} + \left\langle q_n^{\mathcal{U}}\right\rangle\right) - J_n^{\mathcal{R}}\left(\left\langle \psi_n^{\mathcal{U}}\right\rangle, \left\langle q_n^{\mathcal{U}}\right\rangle\right) + \left\langle J_n^{\mathcal{R}}\left(\psi_n^{\mathcal{U}}, q_n^{\mathcal{U}}\right)\right\rangle
\end{aligned} \tag{5.4}$$

Thus we end up with the following expression for the evolution of resolved potential vorticity coefficients:

$$\frac{dq^{\mathcal{R}_n}}{dt} + J^{\text{-}nR}\left(\psi_n^{\mathcal{R}} + \left\langle \psi_n^{\mathcal{U}}\right\rangle, q_n^{\mathcal{R}} + \left\langle q_n^{\mathcal{U}}\right\rangle\right) - J_n^{\mathcal{R}}\left(\left\langle \psi_n^{\mathcal{U}}\right\rangle, \left\langle q_n^{\mathcal{U}}\right\rangle\right) + \left\langle J_n^{\mathcal{R}}\left(\psi_n^{\mathcal{U}}, q_n^{\mathcal{U}}\right)\right\rangle = \nu \nabla \zeta_n^{\mathcal{R}} + \mu(F_n^{\mathcal{R}} - \zeta_n^{\mathcal{R}}) \tag{5.5}$$

We can now evaluate the time evolution of potential vorticity if we have an expression for the expectation value of the unresolved coefficients.

Energy tendency

Anticipating section 5.2 we also derive an expression for the decomposed energy tendency. In (3.16) and (3.17) we now recognize the inner product (4.2) and we can therefore write the energy and its tendency as

$$E = \sum_{n \in \{1,2\}} G_n(-\tfrac{1}{2}\psi_n, q_n) \tag{5.6}$$

$$\frac{d}{dt}E = \sum_{n \in \{1,2\}} G_n\left(-\psi_n, \frac{\partial q_n}{\partial t}\right) \tag{5.7}$$

where we have $G_n = \frac{C}{(2\pi)^2 \Gamma_n}$. The energy can be decomposed in resolved and unresolved parts[3]:

$$E = -\frac{1}{2}\sum_{n \in \{1,2\}} G_n(\psi_n^{\mathcal{R}} + \psi_n^{\mathcal{U}}, q_n^{\mathcal{R}} + q_n^{\mathcal{U}}) = -\frac{1}{2}\sum_{n \in \{1,2\}} G_n(\psi_n^{\mathcal{R}}, q_n^{\mathcal{R}}) - \frac{1}{2}\sum_{n \in \{1,2\}} G_n(\psi_n^{\mathcal{U}}, q_n^{\mathcal{U}}) = E^{\mathcal{R}} + E^{\mathcal{U}} \tag{5.8}$$

In a similar way the energy tendency is treated, and we use (5.2) to get an expression for the unresolved energy tendency in terms of the resolved and unresolved vorticity fields.

$$\begin{aligned}
\frac{dE^{\mathcal{U}}}{dt} &= \sum_{n \in \{1,2\}} G_n\left[-(\psi_n^{\mathcal{U}}, \frac{\partial q_n^{\mathcal{U}}}{\partial t})\right] \\
&= \sum_{n \in \{1,2\}} G_n\left[(\psi_n, J^{\mathcal{U}}(\psi_n^{\mathcal{R}} + \psi_n^{\mathcal{U}}, q_n^{\mathcal{R}} + q_n^{\mathcal{U}})) - \nu(\psi_n^{\mathcal{U}}, \nabla^2 \zeta_n^{\mathcal{U}}) - \mu(\psi_n^{\mathcal{U}}, (F_n^{\mathcal{U}} - \zeta_n^{\mathcal{U}}))\right] \\
&= \sum_{n \in \{1,2\}} G_n\left[(\psi_n^{\mathcal{U}}, J(\psi_n^{\mathcal{R}}, q_n^{\mathcal{R}})) - (\psi_n^{\mathcal{R}}, J(\psi_n^{\mathcal{U}}, q_n^{\mathcal{U}})) - \nu(\zeta_n^{\mathcal{U}}, \zeta_n^{\mathcal{U}}) - \mu(\psi_n^{\mathcal{U}}, (F_n^{\mathcal{U}} - \zeta_n^{\mathcal{U}}))\right]
\end{aligned} \tag{5.9}$$

[2]Note that the Jacobian is a bilinear operator and that the operation of averaging and projecting the Jacobian can be interchanged.
[3]Here we use that our basis functions are orthogonal with respect to the inner product, so there are no cross terms.

A similar expression can be made for the resolved part of the spectrum:

$$\begin{aligned}\frac{dE^{\mathcal{R}}}{dt} &= \sum_{n\in\{1,2\}} G_n\left[-(\psi_n^{\mathcal{R}}, \frac{\partial q_n^{\mathcal{R}}}{\partial t})\right] \\ &= \sum_{n\in\{1,2\}} G_n\left[(\psi_n^{\mathcal{R}}, J(\psi_n^{\mathcal{U}}, q_n^{\mathcal{U}})) - (\psi_n^{\mathcal{U}}, J(\psi_n^{\mathcal{R}}, q_n^{\mathcal{R}})) - \nu(\psi_n^{\mathcal{R}}, \nabla^2\zeta_n^{\mathcal{R}}) - \mu(\psi_n^{\mathcal{R}}, (F_n^{\mathcal{R}} - \zeta_n^{\mathcal{R}}))\right] \\ &= \sum_{n\in\{1,2\}} G_n\left[(\psi_n^{\mathcal{R}}, J(\psi_n^{\mathcal{U}}, q_n^{\mathcal{U}})) - (\psi_n^{\mathcal{U}}, J(\psi_n^{\mathcal{R}}, q_n^{\mathcal{R}})) - \nu(\zeta_n^{\mathcal{R}}, \zeta_n^{\mathcal{R}}) - \mu(\psi_n^{\mathcal{R}}, (F_n^{\mathcal{R}} - \zeta_n^{\mathcal{R}}))\right] \end{aligned} \tag{5.10}$$

Total energy in our system should be conserved apart from the sources and sinks. We see that this holds when we add equations (5.9) and (5.10), because it reduces to the sum of the forcing and viscosity energy terms in both layers.

$$\frac{dE}{dt} = \sum_{n\in\{1,2\}} G_n\left[-\nu(\psi_n, \nabla^2\zeta_n) - \mu(\psi_n, (F_n - \zeta_n))\right] \tag{5.11}$$

To work with (5.9) in our model we need to express the equation in spectral coefficients. With the inner product in spectral space $(\xi, \chi) = \sum_{\boldsymbol{k}} \xi_{\boldsymbol{k}}^* \chi_{\boldsymbol{k}}$. When the inner product is over two equal fields we can take the norm $|\xi|^2$. Written out, (5.9) becomes:

$$\begin{aligned}\frac{dE^{\mathcal{U}}}{dt} = \sum_{n\in\{1,2\}} G_n\Bigg[&\sum_{\mathbf{k}\in\mathcal{U}} \psi_{n,\mathbf{k}}^*(Y_{\mathbf{k}}, J(\psi_n^{\mathcal{R}}, q_n^{\mathcal{R}})) - \sum_{\mathbf{k}\in\mathcal{U}}\sum_{\mathbf{k}'\in\mathcal{U}} \psi_{n,\mathbf{k}}^* q_{n,\mathbf{k}'}(\psi_n^{\mathcal{R}}, J(Y_{\mathbf{k}}, Y_{\mathbf{k}'})) \\ &- \nu\sum_{\mathbf{k}\in\mathcal{U}} |\zeta_{n,\mathbf{k}}|^2 - \mu\sum_{\mathbf{k}\in\mathcal{U}} \psi_{n,\mathbf{k}}^*(F_{n,\mathbf{k}} - \zeta_{n,\mathbf{k}})\Bigg]\end{aligned} \tag{5.12}$$

This can be rearranged by gathering similar terms and using $\mathbf{k}^2\psi_n = -\zeta_n$.

$$\begin{aligned}-\frac{dE^{\mathcal{U}}}{dt} = &\sum_{n\in\{1,2\}}\sum_{\mathbf{k}\in\mathcal{U}} G_n\left[\left(\frac{\mu + \nu\mathbf{k}^2}{\mathbf{k}^2}\right)|\zeta_{n,\mathbf{k}}|^2 + \frac{\chi_{n,\mathbf{k}}}{\mathbf{k}^2}\zeta_{n,\mathbf{k}}^*\right] \\ &- \sum_{n\in\{1,2\}}\sum_{\mathbf{k}\in\mathcal{U}}\sum_{\mathbf{k}'\in\mathcal{U}} G_n\left[\frac{\xi_{n,\mathbf{k},\mathbf{k}'}}{\mathbf{k}^2}\zeta_{n,\mathbf{k}}^* q_{n,\mathbf{k}'}\right]\end{aligned} \tag{5.13}$$

$$\chi_{n,\mathbf{k}} = (Y_{\mathbf{k}}, J(\psi_n^{\mathcal{R}}, q_n^{\mathcal{R}})) - \mu F_{n,\mathbf{k}} \tag{5.14}$$

$$\xi_{n,\mathbf{k},\mathbf{k}'} = (\psi_n^{\mathcal{R}}, J(Y_{\mathbf{k}}, Y_{\mathbf{k}'})) \tag{5.15}$$

We will now make the rather crude approximation to ignore the last term in (5.13). A similar approximation was made by [Verkley et al., 2016] and [Zwaal, 2016] without *a priori* justification. We rely on the numerical *a posteriori* justification of [Zwaal, 2016] that the term is indeed slightly smaller. The main reason for this approximation is to simplify further calculations and reduce computational costs. The expression for the unresolved energy tendency, that will be used to construct the parameterization, has now been reduced to:

$$-\frac{dE^{\mathcal{U}}}{dt} = \sum_{n\in\{1,2\}}\sum_{\mathbf{k}\in\mathcal{U}} G_n\left[\left(\frac{\mu + \nu\mathbf{k}^2}{\mathbf{k}^2}\right)|\zeta_{1,\mathbf{k}}|^2 + \frac{\chi_{n,\mathbf{k}}}{\mathbf{k}^2}\zeta_{n,\mathbf{k}}^*\right] \tag{5.16}$$

5.2 Maximum information entropy

We use the principle of maximum information entropy as conceived by [Jaynes, 2003] to get an expression for the probability density distribution of the spectral coefficients of the unresolved scales. The principle states that, while taking into account all possible distributions under the constraints that form our prior information, the distribution

that is the best representative of our knowledge is the one with maximum entropy. We adopt Jaynes' expression of information entropy S_I of the PDF $\mathcal{P}(\zeta_{\boldsymbol{k}}^{\mathcal{U}})$ [4] and calculate the variation in this quantity due to a change in the PDF.

$$S_I = -\int \mathcal{P}(\zeta_{\boldsymbol{k}}^{\mathcal{U}}) \log \frac{\mathcal{P}(\zeta_{\boldsymbol{k}}^{\mathcal{U}})}{\mathcal{M}(\zeta_{\boldsymbol{k}}^{\mathcal{U}})} d\zeta_{\boldsymbol{k}}^{\mathcal{U}} \qquad \delta S_I = -\int \delta\mathcal{P}(\zeta_{\boldsymbol{k}}^{\mathcal{U}}) \left[\log \frac{\mathcal{P}(\zeta_{\boldsymbol{k}}^{\mathcal{U}})}{\mathcal{M}(\zeta_{\boldsymbol{k}}^{\mathcal{U}})} + 1\right] d\zeta_{\boldsymbol{k}}^{\mathcal{U}}$$

The distribution $\mathcal{M}(\zeta_{\boldsymbol{k}}^{\mathcal{U}})$ represents *a priori* information about the values of the coefficients. Since we have no such information we set it to 1, representing a uniform distribution. We assume two constraints on the distribution: first that it is normalized and second, that the energy transport from and to the unresolved scales is in equilibrium on the timescales of the resolved scales.

$$\langle 1 \rangle = \int \mathcal{P}(\zeta_{\boldsymbol{k}}^{\mathcal{U}}) d\zeta_{\boldsymbol{k}}^{\mathcal{U}} = 1 \qquad \delta \langle 1 \rangle = \int \delta\mathcal{P}(\zeta_{\boldsymbol{k}}^{\mathcal{U}}) d\zeta_{\boldsymbol{k}}^{\mathcal{U}}$$

$$\left\langle \frac{dE^{\mathcal{U}}}{dt} \right\rangle = \int \mathcal{P}(\zeta_{\boldsymbol{k}}^{\mathcal{U}}) \frac{dE^{\mathcal{U}}}{dt}(\zeta_{\boldsymbol{k}}^{\mathcal{U}}) d\zeta_{\boldsymbol{k}}^{\mathcal{U}} = 0 \qquad \delta \left\langle \frac{dE^{\mathcal{U}}}{dt} \right\rangle = \int \delta\mathcal{P}(\zeta_{\boldsymbol{k}}^{\mathcal{U}}) \frac{dE^{\mathcal{U}}}{dt}(\zeta_{\boldsymbol{k}}^{\mathcal{U}}) d\zeta_{\boldsymbol{k}}^{\mathcal{U}}$$

This last assumption is reasonable for most of the resolved scales, although near the truncation the timescale of the resolved scales equals that of the unresolved and the assumption falters. Using Lagrangian multipliers $-\rho$ and α for the constraints we can optimize the information entropy under the constraints by stating

$$\begin{aligned}
0 =& \delta S_I - \rho \delta \langle 1 \rangle + \alpha \delta \left\langle \tfrac{dE^{\mathcal{U}}}{dt} \right\rangle && (5.17)\\
=& -\int \delta\mathcal{P}(\zeta^{\mathcal{U}}) \left[\log \frac{\mathcal{P}(\zeta^{\mathcal{U}})}{\mathcal{M}(\zeta^{\mathcal{U}})} + 1\right] d\zeta^{\mathcal{U}} - \rho \int \delta\mathcal{P}(\zeta^{\mathcal{U}}) d\zeta^{\mathcal{U}} + \alpha \int \delta\mathcal{P}(\zeta^{\mathcal{U}}) \frac{dE^{\mathcal{U}}}{dt}(\zeta^{\mathcal{U}}) d\zeta^{\mathcal{U}} && (5.18)\\
=& -\int \delta\mathcal{P}(\zeta^{\mathcal{U}}) \left[\log \frac{\mathcal{P}(\zeta^{\mathcal{U}})}{\mathcal{M}(\zeta^{\mathcal{U}})} + 1 - \rho + \alpha \frac{dE^{\mathcal{U}}}{dt}\right] d\zeta^{\mathcal{U}} && (5.19)
\end{aligned}$$

Because this expression is true for any $\delta\mathcal{P}(\zeta^{\mathcal{U}})$, the expression between brackets should be zero. This gives, taking $\mathcal{M}(\zeta^{\mathcal{U}}) = 1$,

$$\begin{aligned}
\mathcal{P}(\zeta^{\mathcal{U}}) =& \frac{1}{\mathcal{Z}} \exp\left[\alpha \tfrac{dE^{\mathcal{U}}}{dt}(\zeta^{\mathcal{U}})\right] && (5.20)\\
=& \prod_{\mathbf{k}\in\mathcal{U}} \frac{1}{\mathcal{Z}} \exp \sum_{n\in\{1,2\}} -\alpha G_n \left[\left(\frac{\mu + \nu\mathbf{k}^2}{\mathbf{k}^2}\right) |\zeta_{n,\mathbf{k}}|^2 + \frac{\chi_{n,\mathbf{k}}}{\mu + \nu\mathbf{k}^2} \zeta_{n,\mathbf{k}}^*\right] && (5.21)\\
=& \prod_{n\in 1,2} \prod_{\mathbf{k}\in\mathcal{U}} \frac{1}{\mathcal{Z}} \exp\left[-\alpha G_n \left(\frac{\mu + \nu\mathbf{k}^2}{\mathbf{k}^2}\right) \times \left(|\zeta_{n,\mathbf{k}} + \frac{1}{2}\frac{\chi_{n,\mathbf{k}}}{\mu + \nu\mathbf{k}^2}|^2 - \frac{1}{4}|\frac{\chi_{n,\mathbf{k}}}{\mu + \nu\mathbf{k}^2}|^2\right)\right] && (5.22)\\
=& \prod_{n\in 1,2} \prod_{\mathbf{k}\in\mathcal{U}} \mathcal{N}(\lambda_{n,\boldsymbol{k}}, \sigma_{n,\boldsymbol{k}}, \zeta_{n,\boldsymbol{k}}) && (5.23)
\end{aligned}$$

In the last step we have recognized the multivariate normal distribution

$$\mathcal{N}(\lambda_{n,\boldsymbol{k}}, \sigma_{n,\boldsymbol{k}}, \zeta_{n,\boldsymbol{k}}) = \frac{1}{\sigma_{n,\boldsymbol{k}}^2 2\pi} \exp\left(-\frac{|\zeta_{n,\boldsymbol{k}} - \lambda_{n,\boldsymbol{k}}|^2}{2\sigma_{n,\boldsymbol{k}}^2}\right) \tag{5.24}$$

[4] With $\zeta_{\boldsymbol{k}}^{\mathcal{U}}$ we denote the collection of all coefficients $\zeta_{\boldsymbol{k}}$ where $\boldsymbol{k} \in \mathcal{U}$ and with the distribution $\mathcal{P}(\zeta_{\boldsymbol{k}}^{\mathcal{U}})$ its multivariate probability density function. Consequently an integration over $d\zeta_{\boldsymbol{k}}^{\mathcal{U}}$ concerns a multiple integral over all unresolved coefficients.

and identified the mean, variance and partition function of the distribution.

$$\begin{aligned}\lambda_{n,\boldsymbol{k}} =& -\frac{1}{2}\frac{\chi_{n,\mathbf{k}}}{\mu+\nu\boldsymbol{k}^2}\\ =& -\frac{1}{2}\frac{(Y_{\mathbf{k}}, J(\psi_n^{\mathcal{R}},\zeta_n^{\mathcal{R}})) - \mu F_{n,\mathbf{k}}}{\mu+\nu\boldsymbol{k}^2} \qquad (5.25)\\ \sigma^2_{n,\boldsymbol{k}} =& \frac{1}{2}\frac{\boldsymbol{k}^2}{\alpha G_n}\left(\frac{1}{\mu+\nu\boldsymbol{k}^2}\right) \qquad (5.26)\\ \mathcal{Z} =& \prod_{n\in 1,2}\prod_{\mathbf{k}}\sigma^2_{n,\boldsymbol{k}}2\pi\exp\left(\frac{|\lambda_{n,\boldsymbol{k}}|^2}{2\sigma^2_{n,\boldsymbol{k}}}\right) \qquad (5.27)\end{aligned}$$

5.3 Expectation value

The multivariate normal distribution has some useful properties concerning the expectation values[5]:

$$\begin{aligned}\langle\zeta_{n,\boldsymbol{k}}\rangle =& \lambda_{n,\boldsymbol{k}} \qquad (5.28)\\ \langle\zeta_{n,\boldsymbol{k}}\zeta_{n,\boldsymbol{k}'}\rangle =& \lambda_{n,\boldsymbol{k}}\lambda_{n,\boldsymbol{k}'} + \sigma^2_{\boldsymbol{k}}\delta_{\boldsymbol{k}\boldsymbol{k}'} \qquad (5.29)\\ \langle a\zeta_{n,\boldsymbol{k}} + b\zeta_{n',\boldsymbol{k}'}\rangle =& a\langle\zeta_{n,\boldsymbol{k}}\rangle + b\langle\zeta_{n',\boldsymbol{k}'}\rangle \qquad (5.30)\end{aligned}$$

Returning to equation (5.5) we can write down spectral representation for the expectation values of the fields using the mean of the PDF's. To keep the notation short while expanding q_n, we introduce $m = 3-n$ to represent the other layer than n.

$$\begin{aligned}\left\langle\psi_n^{\mathcal{U}}\right\rangle &= \sum_{\boldsymbol{k}\in\mathcal{U}}\langle\psi_{n,\boldsymbol{k}}\rangle Y_{\boldsymbol{k}} = \sum_{\boldsymbol{k}\in\mathcal{U}} -\frac{\lambda_{n,\boldsymbol{k}}}{\boldsymbol{k}^2}Y_{\boldsymbol{k}} \qquad (5.31)\\ \left\langle\zeta_n^{\mathcal{U}}\right\rangle &= \sum_{\boldsymbol{k}\in\mathcal{U}}\langle\zeta_{n,\boldsymbol{k}}\rangle Y_{\boldsymbol{k}} = \sum_{\boldsymbol{k}\in\mathcal{U}}\lambda_{n,\boldsymbol{k}}Y_{\boldsymbol{k}} \qquad (5.32)\\ \left\langle q_n^{\mathcal{U}}\right\rangle &= \sum_{\boldsymbol{k}\in\mathcal{U}}\langle q_{n,\boldsymbol{k}}\rangle Y_{\boldsymbol{k}} = \sum_{\boldsymbol{k}\in\mathcal{U}}\left\langle\zeta_{n,\boldsymbol{k}} + \frac{\Gamma_n}{\boldsymbol{k}}(\zeta_{m,\boldsymbol{k}} - \zeta_{n,\boldsymbol{k}})\right\rangle Y_{\boldsymbol{k}}\\ &= \sum_{\boldsymbol{k}\in\mathcal{U}}\left(\langle\zeta_{n,\boldsymbol{k}}\rangle + \frac{\Gamma_n}{\boldsymbol{k}^2}(\langle\zeta_{m,\boldsymbol{k}}\rangle - \langle\zeta_{n,\boldsymbol{k}}\rangle)\right)Y_{\boldsymbol{k}} = \sum_{\boldsymbol{k}\in\mathcal{U}}\left(\lambda_{n,\boldsymbol{k}} + \frac{\Gamma_n}{\boldsymbol{k}^2}(\lambda_{m,\boldsymbol{k}} - \lambda_{n,\boldsymbol{k}})\right)Y_{\boldsymbol{k}} \qquad (5.33)\end{aligned}$$

We get for the term $\left\langle J^{\mathcal{R}}\left(\psi_n^{\mathcal{U}}, q_n^{\mathcal{U}}\right)\right\rangle$ in (5.5) in spectral representation:

$$\begin{aligned}\left\langle J^{\mathcal{R}}\left(\psi_n^{\mathcal{U}}, q_n^{\mathcal{U}}\right)\right\rangle =& -\sum_{\boldsymbol{k}\in\mathcal{U}}\sum_{\boldsymbol{k}'\in\mathcal{U}} J(Y_{\boldsymbol{k}}, Y_{\boldsymbol{k}'})\langle\psi_{n,\boldsymbol{k}}q_{n,\boldsymbol{k}'}\rangle\\ =& \sum_{\boldsymbol{k}\in\mathcal{U}}\sum_{\boldsymbol{k}'\in\mathcal{U}}\frac{J(Y_{\boldsymbol{k}}, Y_{\boldsymbol{k}'})}{\boldsymbol{k}^2}\left\langle\zeta_{n,\boldsymbol{k}}\left(\zeta_{n,\boldsymbol{k}'} + \frac{\Gamma_n}{\boldsymbol{k}'^2}(\zeta_{m,\boldsymbol{k}'} - \zeta_{n,\boldsymbol{k}'})\right)\right\rangle\\ =& \sum_{\boldsymbol{k}\in\mathcal{U}}\sum_{\boldsymbol{k}'\in\mathcal{U}}\frac{J(Y_{\boldsymbol{k}}, Y_{\boldsymbol{k}'})}{\boldsymbol{k}^2}\lambda_{n,\boldsymbol{k}}\left(\lambda_{n,\boldsymbol{k}'} + \frac{\Gamma_n}{\boldsymbol{k}'^2}(\lambda_{m,\boldsymbol{k}'} - \lambda_{n,\boldsymbol{k}'})\right)\\ =& J^{\mathcal{R}}\left(\left\langle\psi^{\mathcal{U}}\right\rangle, \left\langle q^{\mathcal{U}}\right\rangle\right) \qquad (5.34)\end{aligned}$$

Where we have used eqs. (5.29) and (5.30) in the third step, together with the fact that the second part of eq. (5.29) is only nonzero in case of equal $\boldsymbol{k}$ in which case $J(Y_{\boldsymbol{k}}, Y_{\boldsymbol{k}'})$ is zero. Because of this equality we can reduce eq. (5.5) to:

$$\frac{dq^{\mathcal{R}}}{dt} + J^{\mathcal{R}}\left(\psi^{\mathcal{R}} + \left\langle\psi^{\mathcal{U}}\right\rangle, q^{\mathcal{R}} + \left\langle q^{\mathcal{U}}\right\rangle\right) = \nu\nabla\zeta^{\mathcal{R}} + \mu(F^{\mathcal{R}} - \zeta^{\mathcal{R}}) \qquad (5.35)$$

The parameterization now consists of replacing $\left\langle\psi^{\mathcal{U}}\right\rangle$ in this equation using eqs. (5.14), (5.25) and (5.31),

[5]The third property is not unique to a normal distribution but is true for any probability distribution.

$$\begin{aligned}\left\langle \psi_n^{\mathcal{U}} \right\rangle &= \sum_{\boldsymbol{k}\in\mathcal{U}} -\frac{\lambda_{n,\boldsymbol{k}}}{\boldsymbol{k}^2} Y_{\boldsymbol{k}} \\ &= \sum_{\boldsymbol{k}\in\mathcal{U}} \frac{1}{2} \frac{(Y_{\mathbf{k}}, J(\psi_n^{\mathcal{R}}, \zeta_n^{\mathcal{R}})) - \mu F_{n,\mathbf{k}}}{\boldsymbol{k}^2(\mu + \nu\boldsymbol{k})} Y_{\boldsymbol{k}}\end{aligned} \tag{5.36}$$

and likewise for $\left\langle q^{\mathcal{U}} \right\rangle$, where the conversion from and $\left\langle \psi^{\mathcal{U}} \right\rangle$ to and $\left\langle q^{\mathcal{U}} \right\rangle$ follows from eq. (4.5) and section 4.2.

Chapter 6

Results

This chapter discusses the experimental setup and diagnostic techniques and presents the results.

6.1 Experimental setup

The attempt to obtain stable turbulent flow fields resulted in parameters that were not deduced from physical systems but could produce a steady flow field with enough detail and at the same time contain the phenomena that make the quasi-geostrophic system interesting. With this tuning process, we ended up with system parameters as in **??**. Even though no units were introduced into the equations that define the quasi-geostrophic model, we have made several assumptions that put constraints on the model parameters. We know that the Rossby number must be in the order of 0.1 and Γ_n is in the order of the inverse Rossby number. We choose Γ_1 to be 1.5 times Γ_2 and $\Gamma_1 + \Gamma_2 = \frac{1}{Ro}$, so we get $\Gamma_1 = 6$ and $\Gamma 2 = 4$. The Coriolis variation was chosen to be $\frac{1}{2}$, which produced a westward drift of the flow field yet the system could still become turbulent.
The viscosity coefficient was chosen such that a vorticity wave at the highest simulated wavenumber damps with an e-folding time of 5 simulation time units. Here we use non-dimensional time units of $\frac{1}{\Omega}$ with Ω being earth's angular velocity $\Omega = 7.292 \cdot 10^{-5}\mathrm{s}^{-1}$ to express our simulation time in days[1]. The linear forcing and damping term was scaled with μ to accomplish an e-folding time of 90 days.

$$\nu = \frac{1}{5 \cdot 24 \cdot 60 \cdot 60} \frac{1}{\Omega} \frac{1}{N^2} = \frac{6.34 \cdot 10^{-2}}{N^2} \tag{6.1}$$

$$\mu = \frac{1}{90 \cdot 24 \cdot 60 \cdot 60} \frac{1}{\Omega} = 1.76 \cdot 10^{-3} \tag{6.2}$$

where N is the highest wavenumber in the simulation. To get the system in a statistical equilibrium we needed to tune the forcing amplitude. A random forcing field was applied in the first layer, where the tunable parameter determined the maximum amplitude of the forcing modes.
Each experiment compares the three different types of parameterizations with each other and a reference run as listed in table 6.1. The reference run is performed at a model resolution of 256 as opposed to the parameterized models which were truncated at a resolution of 128 spectral modes. The cutoff in the reference run has negligible effect on the scales at the cutoff region in the truncated runs. In this sense we refer to the reference run as the "truth". Although we only calculate 128 spectral modes, the parameterizations and truncated experiment run at full resolution to keep the viscosity and other resolution dependent terms the same.
The simulations performs 200 integration steps per time unit. We start all four runs with the same initial field. This field is produced using a spin up run at full resolution starting from an all-zero vorticity field until the system reaches a state of statistical equilibrium. The energy spectrum stabilizes after approximately 500 simulation days.

[1] Note that this does not necessarily mean that a time unit is equal to an earth day. We still have a very non-geophysical model with non-physical forcing and damping terms and it would be wrong to say that a time unit represents a day in the earth's atmosphere.

Run Type	Resolution	Parameterization
Full res.	256	None
Not par.	128	None
Inc. vis.	128	Increased Viscosity
Max. ent.	128	Maximum Entropy

Table 6.1: Scheme of runs in each experiment

6.2 Vorticity fields

Serving as a first visual qualitative diagnostic, the vorticity fields were obtained from the simulations' spectral fields by performing a Fourier transformation back to grid point space. The animated vorticity fields show the expected behavior of a quasi-geostrophic system. We see a clear beta-plane propagation to the left and we can discern Rossby waves in the flow field. In section 6.2 the flow fields of the three parameterizations and the reference run can be found for successive times after initialization using a spun up vorticity field. The images are sampled at 20, 70 and 120 days after initialization. We see that all simulations maintain a flow pattern similar to the full resolution run even after 120 days. We found that this remained so for the rest of the simulation which is an interesting property since the fields, although sharing the same initial field, run independent from the reference run and should lose their correlation after considerable time. We do note that the structure of the fields is different for the for runs. The full resolution run naturally has the most detail. The maximum entropy run resembles this detail very well, while the unparameterized run has a grainy texture due the energy cascade which encounters a impenetrable wall at the truncation. Energy heaps up at those small scales, causing the grainy texture. The high viscosity run seems more smeared out, thereby losing the grainy texture we see in unparameterized run, but also losing the small details. If we look closely at the encircled vortex in the $t = 120$ series, we see the effect of the different types of parameterizations and the fact that the unparameterized run and high viscosity run have distorted this vortex considerably more than in the maximum entropy run, which conserves many of the small details from the full resolution.

6.3 Field correlation

For quantitative comparison of the forecast skill of the three simulations, the sample Pearson correlation coefficient of the vorticity fields can be computed. We consider the collection of vorticity values of all N grid points of a single time step as a sample. For an experiment E and reference run R, the correlation coefficient is then given by:

$$\rho = \frac{\sum_{i=1}^{N}(E_i - \overline{E})(R_i - \overline{R})}{\sqrt{\sum_{i=1}^{N}(E_i - \overline{E})^2} \times \sqrt{\sum_{i=1}^{N}(R_i - \overline{R})^2}} \tag{6.3}$$

This coefficient is calculated for the three models with the full resolution run as reference run at every 10 days. As this is bound to give a rather noisy time evolution, the experiment was done for a small ensemble of five runs starting from various initial fields. These initial fields are obtained by a long (40000 days) run on full resolution and sampling new initial fields every 5000 days. By the chaotic nature of turbulent flow, these fields will be statistically uncoupled. A similar approach has been followed in previous research on this parameterization [Kalverla, 2015]. The results for the full time series of layer 1 are shown in fig. 6.2a and truncated versions for both layers in figs. 6.2b and 6.2c.

It can be seen that the maximum entropy parameterization improves over the unparameterized run in the first 120 days, while the increased viscosity performs worst. At approximately 150 days, the models become equally correlated and remain fluctuating around a correlation coefficient of 0.5. The fields thus remain highly correlated, even when they should be decoupled from the reference run. An explanation lies probably in the random forcing that has the same time evolution in all runs. If this random forcing is too strong, the fields will constantly be correlated strongly to the forcing field. To check this hypothesis, short ensemble runs were done with different random seeds. The correlation coefficient for these runs dropped within several time units to zero, confirming the strong influence of the forcing field.

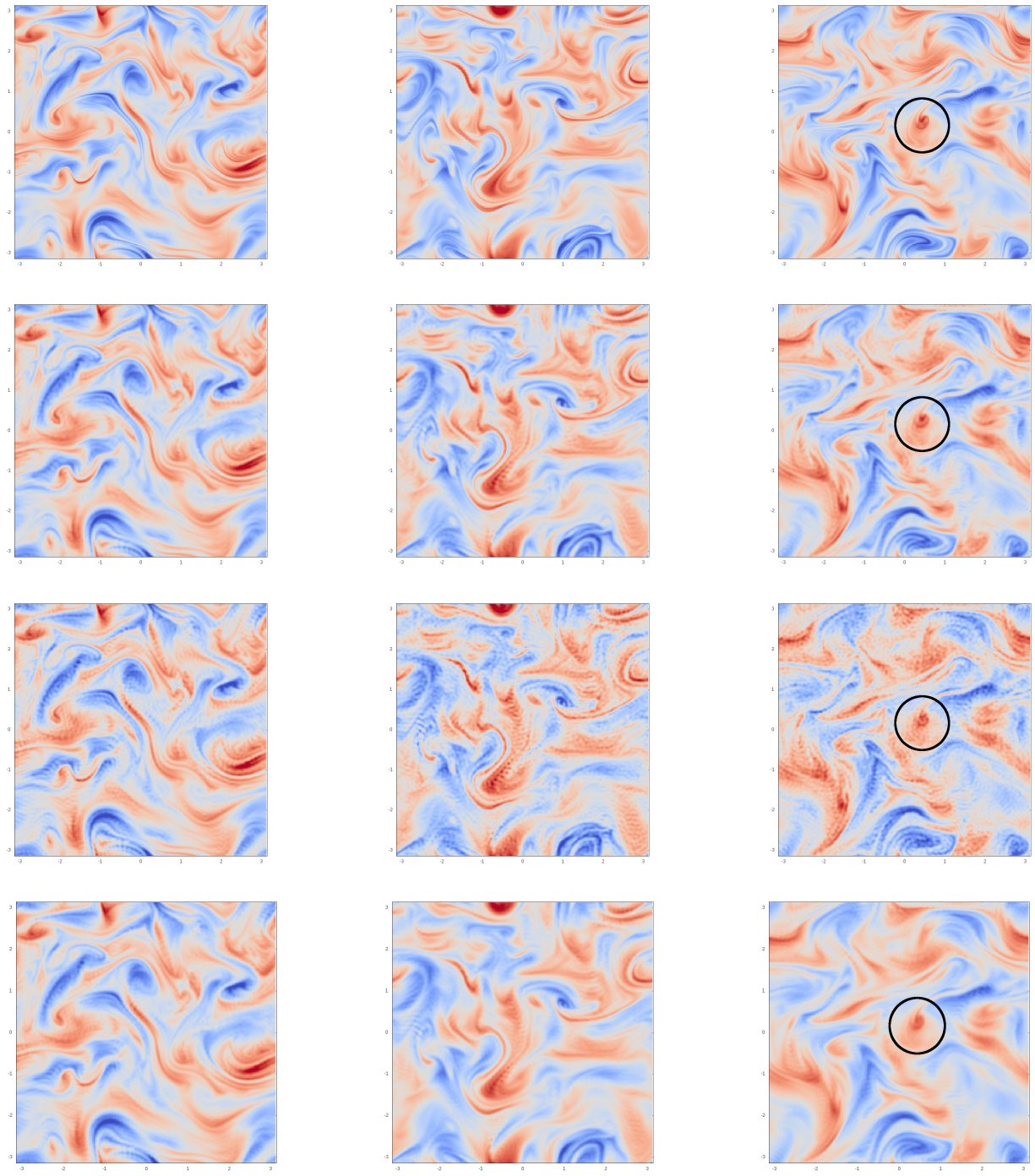

(a) t=20 (b) t=70 (c) t=120

Figure 6.1: Short times series of the states of all four runs. From top to bottom we have : (1) Full resolution, (2) Maximum entropy parameterization, (3) Not parameterized, (4) High viscosity parameterization.

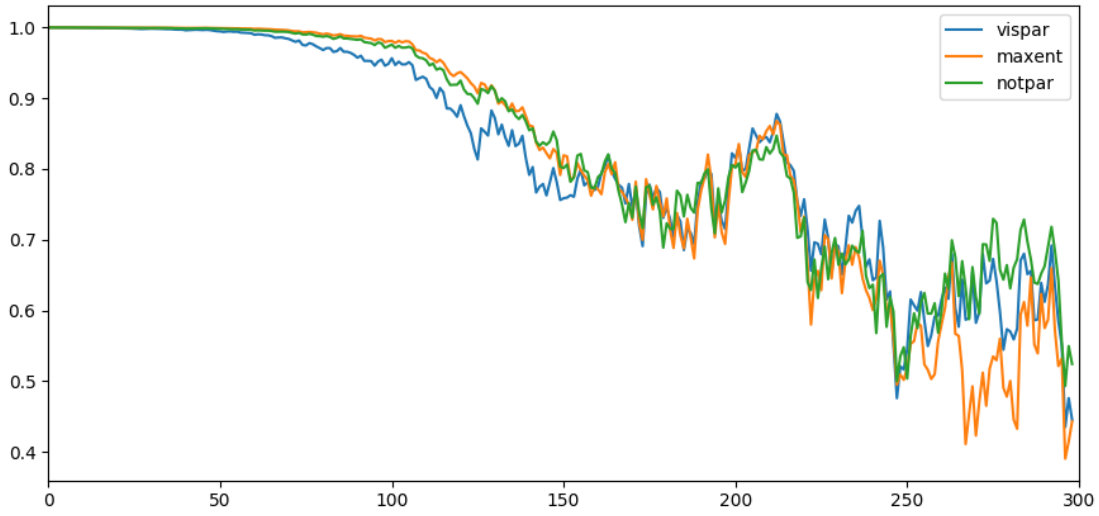

(a)

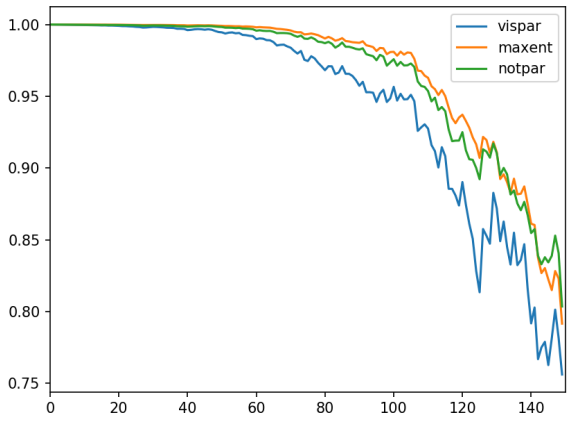

(b)

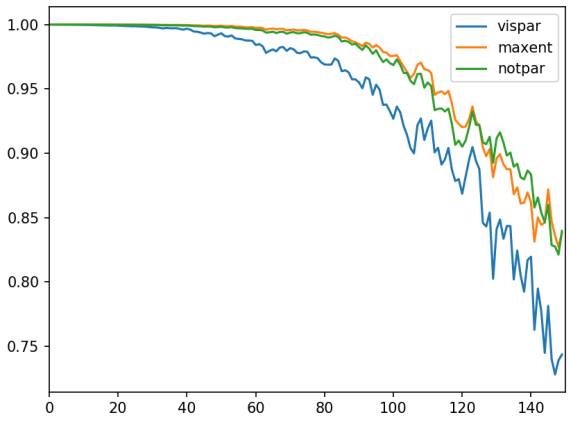

(c)

Figure 6.2: (a) The correlation coefficient (ρ) of layer 1 over the full time span; (b) and (c) the correlation coefficient of respectively layer 1 and 2, truncated to contain the part of the time series until the forcing correlation is reached.

6.4 Kinetic energy and enstrophy spectra

The kinetic energy or enstrophy spectrum of the flow field can be calculated by summing up the contributions from all spectral coefficients for which $k_b - \frac{1}{2} \leqslant \sqrt{\boldsymbol{k}^2} < k_b + \frac{1}{2}$ in bins for positive integers k_b. There is however a non homogeneous distribution of spectral coefficients over these bins because of the rectangular discrete grid combined with the circular summation of contributions. The bins can be corrected for this artifact by a division by the weight $w(k_b) = N_{k_b}/(2\pi k_b)$, where N_{k_b} is the number of grid points that fall within in each bin.

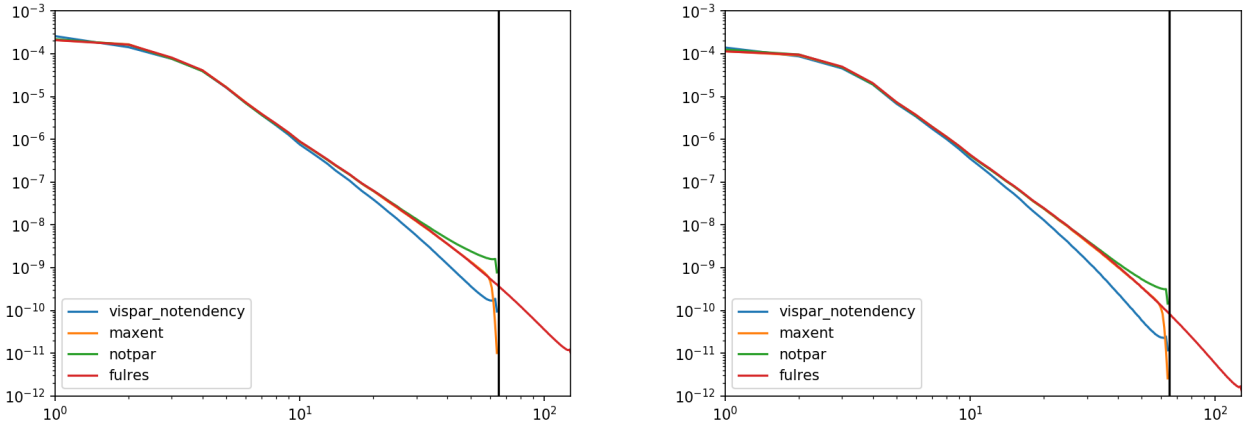

(a) (b)

Figure 6.3: The mean kinetic energy spectrum for layer 1 (a) and layer 2 (b) over a 10000 day run, sampled at each 10 steps.

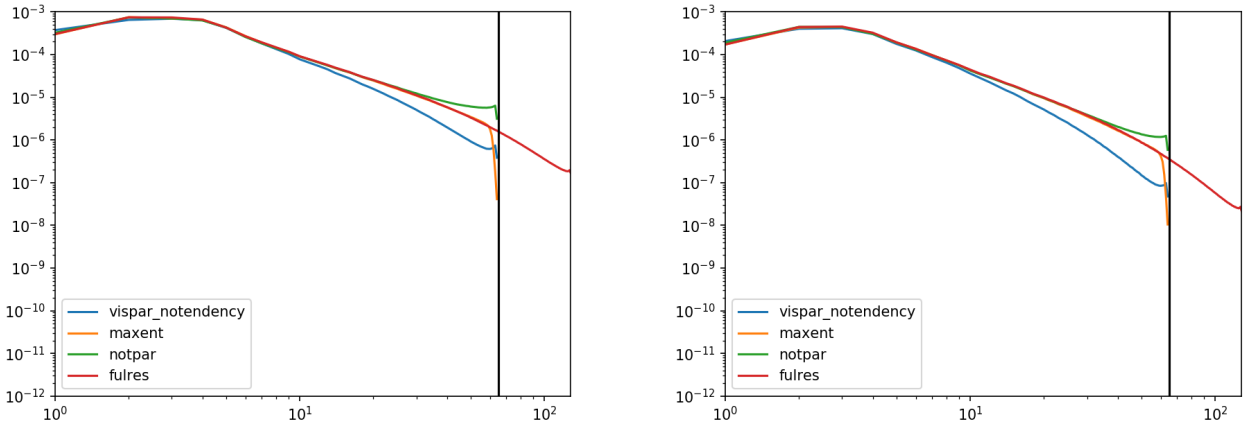

(a) (b)

Figure 6.4: The mean enstrophy spectrum for layer 1 (a) and layer 2 (b) over a 10000 day run, sampled at each 10 steps.

For the spectra in figs. 6.3 and 6.4, we see that the maximum entropy run resembles the reference run the most. The unparameterized run has too much kinetic energy in the small scales, since the forward energy scattering can not continue beyond the truncation. The high viscosity parameterization, on the other hand, estimates the kinetic

energy at small scales far too low. Only at a few wave numbers before the truncation does the maximum entropy spectrum diverge from the reference run spectrum.

6.5 Thuburn energy transfer spectra

The energy and enstrophy transport from the unresolved scales to resolved scales due to the nonlinear terms was computed using the diagnostic of [Thuburn et al., 2013]. It was slightly altered to be applied to a two layer quasi-geostrophic model. This shows how well the parameterization mimics the nonlinear processes that transfer energy from unresolved to resolved scales. We can compute the energy tendency for a given wave number k by $\frac{dE_{\boldsymbol{k}}}{dt}$. We can do this for all wave numbers, denoted by $\dot{E}_{\boldsymbol{k}}$, or only the resolved ones $\dot{E}^{\mathcal{R}}_{\boldsymbol{k}}$. Now it is easy to calculate the energy transfer due to the unresolved scales by $\dot{E}^{\mathcal{U}}_{\boldsymbol{k}} = \dot{E}_{\boldsymbol{k}} - \dot{E}^{\mathcal{R}}_{\boldsymbol{k}}$ and we can construct a spectrum in the same way as in section 6.4. The same can be done for the enstrophy transfer and both spectra are shown for the reference, increased viscosity and maximum entropy run in section 6.5. The unparameterized transfer spectrum is by definition zero.

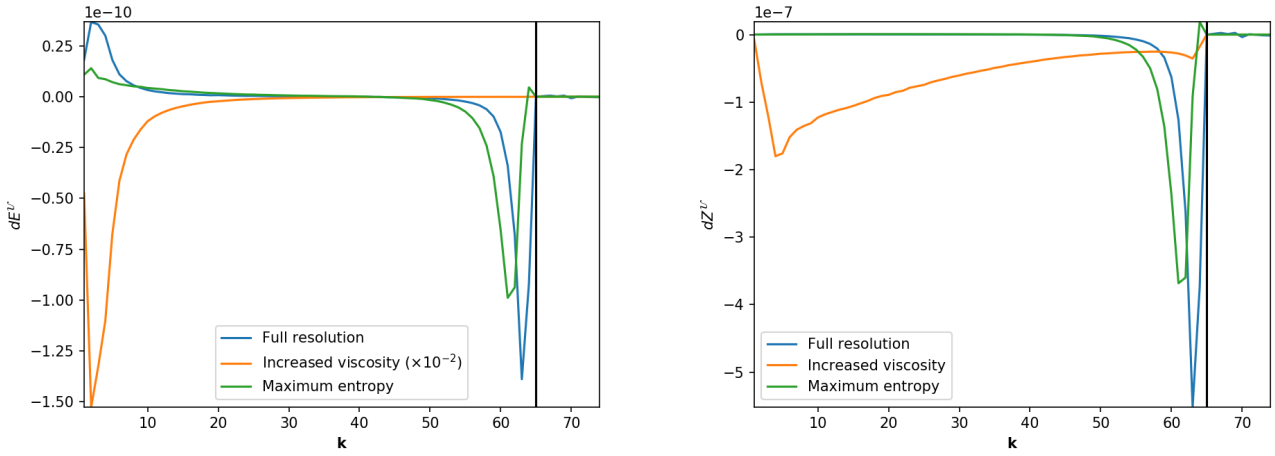

(a) (b)

Figure 6.5: The total energy tendency from the unresolved to the resolved scales. Negative values means energy is drained to the unresolved scales. We also see the backscatter for the full resolution and maximum entropy run at small wavenumber. The energy transfer spectrum of the increased viscosity run had to be scaled with a factor of 10^{-2}.

We see that the maximum entropy run resembles the full resolution run best and the backscatter process is present as we see from the small peak at large scales. Although both the forward scatter as backscatter effect is too small in the maximum entropy run. The increased viscosity run shows no backscatter, but a large drain of energy from larges scales. This excessive drain is due to the large amount of energy in the large scales as we saw from fig. 6.3, together with the simple form of the parameterization. The parameterization is not able to extract enough energy from small scales while leaving the large scales untouched. The maximum entropy parameterization on the other hand manages to mimic the reference transfer.

6.6 Climate

To analyze the long term statistical values, the measurements of long runs of 10000 days were averaged over time to give the so called model climate diagnostics. The mean and variance of the total energy were calculated by summing all contributions at every 10 days and averaging over the number of samples. A normal distribution could then be drawn with the given mean and variance. This was done for each of the models for total energy and enstrophy comparison.

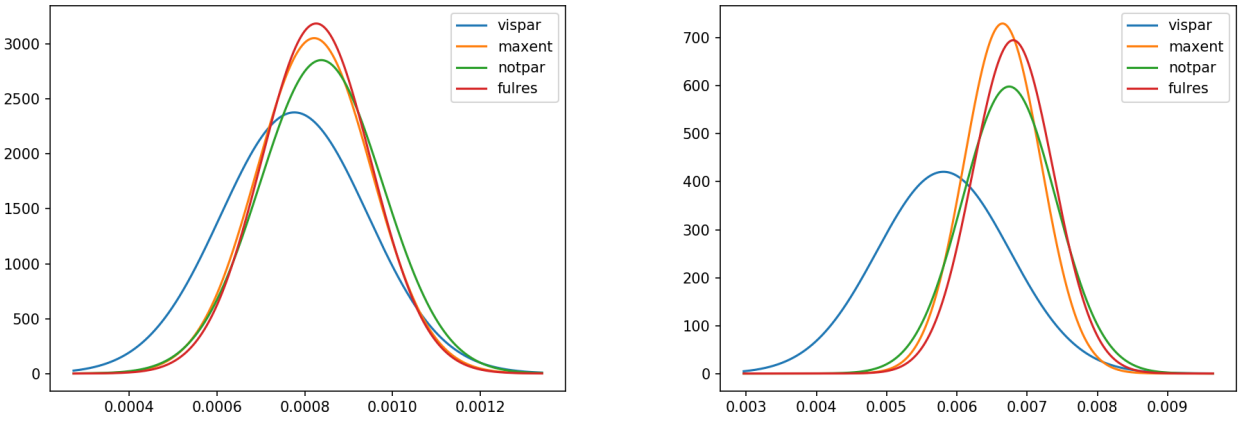

(a) (b)

Figure 6.6: Statistical distributions of the total energy and enstrophy for all models, obtained by plotting a normal distribution with mean and variance of the total energy and enstrophy over time.

We see again that the maximum entropy mean total energy and enstrophy distributions resemble the reference run best. The difference is however not as convincing as in [Verkley et al., 2016]. Especially the difference between the unparameterized run and the maximum entropy parameterization is almost neglegible. This is again probably due to the high forcing field that correlates the fields too strong and has a large impact on the energy of the system.

Chapter 7

Discussion and conclusions

In general it was found that the performance of the maximum entropy parameterization in the two-dimensional quasi-geostrophic domain was an improvement over the unparameterized version and the increased viscosity model. However the results are not conclusive and the system should be tested more for different flow regimes and model parameters. More specific, the flow fields seem to remain similar to the reference run over time and the evaluation of the correlation coefficient confirms this. After a short decline that is slowest for the maximum entropy parameterization, all models settle in a strongly fluctuating correlation around 0.5. This was ascribed to the high forcing and a check on this hypothesis by correlating with a reference run with different forcefields shows a steep decline within several time units to a zero correlation. The average spectra show more promising results, as we see a clear deviance from the reference run for the unparameterized and increased viscosity run and a good correspondence until the last few modes before the truncation. The energy transfer spectra were show even clearer evidence as the specific shape of the transfer spectra almost equal for the reference and maximum entropy run, only the amplitude was too low for the maximum entropy parameterization. The increased viscosity shows a strong drain in the large scales, which is the contrary of the backscatter in the reference run. Finally the climate statistics were not very convincing due to the fluctuations in and strong coupling to the random forcing field. Some remarks can be made on the research and suggestions for further research are done.

7.1 Computational expense

If we compute the order of computational complexity for this simulation we only take into account the bottleneck of the computation which is the calculation of the Jacobian matrices. In the current implementation this is done via the pseudo-spectral method, involving two Fast Fourier transforms ($\mathcal{O}(N \log N)$) and the Jacobian computation in grid space ($\mathcal{O}(N^2)$). So for an unparameterized run we have at the moment a complexity of $2 \times \mathcal{O}(N \log N) + \mathcal{O}(N^2) = \mathcal{O}(N^2)$ where N is the number of grid points. For a parametrized run this is of order $2(N_P)^2$ because the Jacobian should be calculated twice for a truncated number of grid points N_P. For the parametrized simulation with given number of grid points N_P to be of any use, it should qualitatively outperform a non-parametrized run with a number of grid points approximately equal to:

$$N \approx \sqrt{2} N_P \tag{7.1}$$

No actual measurements of computational times for the runs of this research were made since all models had to be run on full resolution even though $\frac{3}{4}$ of the domain was set to 0 at each step to imitate the truncation. The Jacobian was calculated on full resolution in each step. This was done because several model parameters depend on the resolution and since we wanted to compare the different models while model parameters could remain unchanged. Since the investigation of this parameterization is still in an experimental stadium, the efficiency of the computation is not yet of concern, as the principle on which the parameterization is built should first be checked to be correct. However, the reason to parameterize a model is to reduce computational times as opposed to a higher resolution unparameterized run with the same predictive ability. Improvements on the parameterization method could be made by only calculating the most important part of the spectrum, which is near the truncation and at the very large scales, as can be seen from the Thuburn transfer spectra. Together with the symmetry of the Jacobian in spectral space it could be more efficient to abandon the pseude-spectral method and keep the Jacobian computation

in spectral space. The large range in between the two peaks could be skipped in the computation. The question whether this parameterization actually has the potential of reducing this time remains a substantial one and should be looked into.

7.2 Improvement over conventional parametrization

A supplementary requirement of the new parameterization is that it is an improvement over other parameterizations that are, in most cases, less expensive to run. In this report the maximum entropy method has only been compared to a simple increased eddy viscosity run, which has a runtime equal to a run that is not parameterized and only truncated. It was found that the increased viscosity parameterization in its current state performs much worse than either the full resolution run and the maximum entropy parameterization. A concerning fact however is that the increased viscosity parameterization even performs worse than the unparameterizated run in all diagnostics. Also [Kalverla, 2015],[Verkley et al., 2016] and [Zwaal, 2016] show the same behavior for this parameterization. This is a strong indicator that the comparison with this conventional parameterization is not fair. The viscosity can of course be tuned to perform better and a comparison could be made with a tuned viscosity model. More intelligent schemes exist, like the ones proposed by [Thuburn et al., 2013], and should be included in the comparison in future research. In comparing the maximum entropy parameterization with other parameterizations it should always be noted however that while other models should always be tuned to a certain domain and simulation parameters, the maximum entropy parameterization is not tunable and adapts itself to the domain.[1]

7.3 Model parameters

The experiments that were performed in this research were not chosen to reproduce a true geophysical system but only to test the concept of the parameterization on the two-layer quasi-geostrophic system. However it was found that the model is in fact very sensitive to some of its parameters and these should be chosen with care. To produce a detailed flow field, the viscosity coefficient ν had to be small enough. For having a too high value would result in too strong damping of the applied forcing to transfer energy to smaller scales. A too high value for Coriolis variation β would result in a purely zonal flow, and also no small structure. For given system parameters, the forcing had to be of sufficient strength to produce an interesting flow field.
The remarkable fact that the correlation coefficient does not converge towards zero but remains fluctuating around 0.5 for all runs could be ascribed to an inconvenient choice of parameters. The effect is probably due to a relatively high forcing. The forcing, being identical in all models, inevitably introduces a correlation between the different models. The high forcing was needed to produce a turbulent state with the chosen viscosity coefficient. Due to this choice of parameters the diagnostics of the experiments are not as convincing as they could be. Given this result, the parameters could be tuned again to produce a turbulent flow with less applied forcing.

[1] There seems to be a caveat to this, as recent experiments on high resolution have shown that also a energy constraint is needed for the parameterization to perform well. The energy budget then becomes the tunable parameter for this parameterization.

Bibliography

[Cavallini and Crisciani, 2013] Cavallini, F. and Crisciani, F. (2013). *Quasi-Geostrophic Theory of Oceans and Atmosphere*. Springer.

[Crommelin and Verheul, 2016] Crommelin, D. and Verheul, N. (2016). Data-driven stochastic representations of unresolved features in multiscale models. *Communications in Mathematical Sciences*.

[Cushman-Roisin and Beckers, 2009] Cushman-Roisin, B. and Beckers, J.-M. (2009). *Introduction to geophysical fluid dynamics*. Acedemic Press.

[Duchene, 2014] Duchene, V. (2014). On the rigid-lid approximation for two shallow layers of immiscible fluids with small density contrast. *Journal of Nonlinear Science*.

[Jaynes, 2003] Jaynes, E. (2003). *Probability Theory, The logic of science*. Cambridge University Press, Cambridge, U.K.

[Kalverla, 2015] Kalverla, P. (2015). A maximum entropy approach to the parameterization of subgrid-scale processes in two-dimensional flows. Master's thesis, Wageningen University.

[Orszag, 1970] Orszag, A. (1970). Transform method for the calculation of vector-coupled sums: Application to the spectral form of the vorticity equation. *Journal of the Atmospheric Sciences*.

[Thuburn et al., 2013] Thuburn, J., Kent, J., and Wood, N. (2013). Cascades, backscatter and conservation in numerical models of two-dimensional turbulence. *Quarterly Journal of the Royal Meteorological Society*, 140(626).

[Vallis, 2006] Vallis, G. K. (2006). *Atmospheric and Oceanic Fluid Dynamics*. Cambridge University Press, Cambridge, U.K.

[Verkley, 2000] Verkley, W. T. M. (2000). On the vertical velocity in an isentropic layer. *Quarterly Journal of the Royal Meteorological Society*, 126:263 – 274.

[Verkley et al., 2016] Verkley, W. T. M., Kalverla, P. C., and Severijns, C. A. (2016). A maximum entropy approach to the parametrization of subgrid processes in two-dimensional flow. *Quarterly Journal of the Royal Meteorological Society*, 142(699):2273–2283.

[Zwaal, 2016] Zwaal, B. (2016). A maximum entropy parameterization for two-dimensional turbulence. Master's thesis, University of Amsterdam.